

53-27-27
NACA TN 2952

NATIONAL ADVISORY COMMITTEE FOR AERONAUTICS



TECHNICAL NOTE 2959

THEORETICAL INVESTIGATION OF THE SUPERSONIC LIFT
AND DRAG OF THIN, SWEPTBACK WINGS WITH
INCREASED SWEEP NEAR THE ROOT

By Doris Cohen and Morris D. Friedman

Ames Aeronautical Laboratory
Moffett Field, Calif.



Washington
June 1953

AFL 2011
TECHNICAL NOTE 2959
AFL 2011

319.98/9



0065958

1E

NATIONAL ADVISORY COMMITTEE FOR AERONAU

TECHNICAL NOTE 2959

THEORETICAL INVESTIGATION OF THE SUPERSONIC LIFT

AND DRAG OF THIN, SWEPTBACK WINGS WITH
INCREASED SWEEP NEAR THE ROOT

By Doris Cohen and Morris D. Friedman

SUMMARY

Formulas are derived by the use of linearized theory for the lift and drag due to lift, at supersonic speeds, of thin, flat wings having a discontinuity in the leading-edge sweep, the inboard portion of the leading-edge being very highly swept and the outboard portion less so. Examples are presented to show the effect of the bend in the leading edge on the pressure distribution. The lift-curve slope and drag have been calculated for several families of wings, all with straight trailing edges. For two typical plan forms, the aerodynamic-center location has been calculated through a limited range of supersonic Mach numbers.

The over-all characteristics of the wings studied show little effect of the concentration of sweep near the root, in the absence of thickness and viscosity, but appear to be determined primarily by the sweep of the outer portion. However, there is a shift of the lifting pressure away from the central portion of the wing and toward the leading edge of the outer portions. In most cases, there will also be a region of high lift around the trailing edge of the root section. As a result, the aerodynamic center is generally farther back than on comparable conventional wings. In the limited calculations made, no shift of aerodynamic-center location with Mach number was observed. Similar effects are to be expected on the wing of a wing-fuselage configuration of similar plan form.

INTRODUCTION

Considerable interest has been shown in the use of wing plan forms incorporating a region of increased leading-edge sweep, similar to a large fillet, near the wing root. The forward extension of the root chord can provide both increased wing depth, with its structural

advantage, and a useful and accessible volume for the installation of fixed equipment, fuel, air scoops, or complete power plants, depending upon the airplane size and purpose. Such a wing plan form should be particularly useful for an all-wing airplane because of the greater flexibility allowed in the chordwise location of the major weight items.

The use of a so-called "cranked" or "crescent" plan form also has several potential aerodynamic advantages.¹ Theoretical considerations indicate that the low-speed stability and control characteristics should be improved and the high-speed wave drag reduced by increasing the sweep near the root and decreasing it near the tips. Early attempts to realize these advantages resulted in the experimental wings reported in references 1 and 2. The wings did, in fact, show good maximum lift and aileron effectiveness at low speeds, although no extensive comparison was made with conventional swept wings. Reduction in form drag at high subsonic speeds was achieved because the wing chord was increased without increasing the thickness.

As far as is known at this time, no investigation has been made into the supersonic characteristics of the cranked wing. The present report considers the theoretical forces and moments on such wings due to angle of attack, for speeds greater than the speed of sound. In order to reduce the number of variables, the wing plan form has been kept as simple as possible. In every case, the trailing edge is unswept. A single bend is introduced into the leading edge at various locations, and various amounts of sweepback are specified for the inner and outer portions. The sweep of the inner portion of the wings is always high enough so that the forepart of the wing lies inside the Mach cone from its apex. Finally, the wings considered have tips either tapered to a point (type A of fig. 1) or cut off in the streamwise direction (type B). The distribution of lift, the total lift, and the drag due to lift are derived using linearized supersonic wing theory, and some investigation of the aerodynamic-center location is made.

The applicability of the results to the all-wing airplane with thickened and lengthened root section has been mentioned. The results should offer, also, at least a qualitative indication of the distribution of pressures to be expected on the wing of a wing-fuselage combination of similar plan form, particularly if the fuselage has a flattened cross section. For information bearing on this point, the reader is referred to a paper by Morikawa (ref. 3).

¹Both structural and aerodynamic considerations behind the selection of the crescent wing are discussed in an article by R. S. Stafford in the British publication, *The Aeroplane*, Jan. 2, 1953, pp. 6-7.

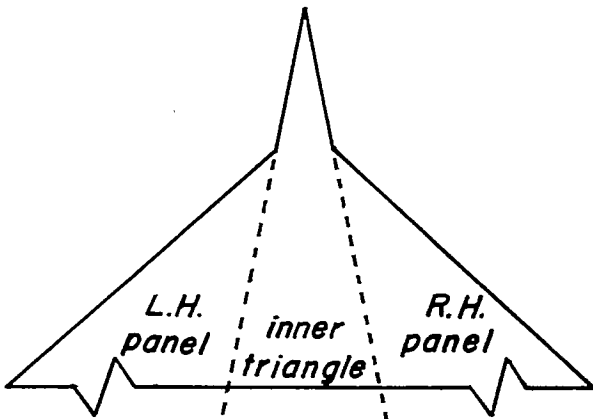
METHOD OF ANALYSIS

Approach to the Problem

The method of analysis will be described in some detail, since it is applicable to a more general class of wing than is discussed here. Basically, the method consists of the superposition of solutions of the linearized supersonic-flow equations. For the most part, conical-flow solutions will be employed, in the manner suggested by Busemann (ref. 4) and Lagerstrom (ref. 5). The method of Mirels (ref. 6) will also be used, however.

Consider first wing A. Nothing that occurs behind its trailing edge can affect the flow over the wing itself (since small perturbations are assumed). Hence, it is permissible to ignore temporarily the position of the trailing edge, that is, to assume that the wing extends to infinity both laterally and to the rear. Now consider the infinite triangle formed by the downstream extension of the inner portions of the leading edge. (See sketch (a).) The complete solution for such a triangle flying as an isolated wing is, of course, known (refs. 7, 8, and 9). However, the accompanying upwash on either side of the triangle violates the requirement of tangential flow over the outer panels of the complete wing. We therefore superimpose additional solutions of the supersonic flow equations which have the property of "canceling" the upwash within the area of the horizontal plane occupied by the outer panels, without introducing any new vertical velocities through the region occupied by the center triangle.

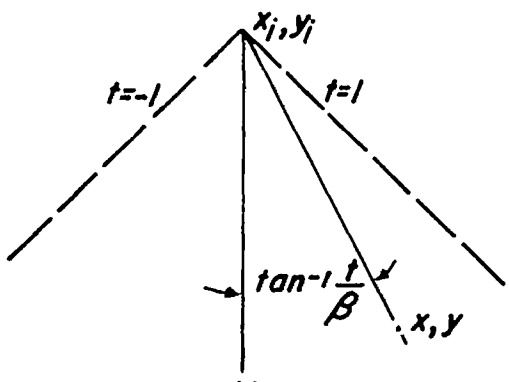
This step determines that the flow will conform to the condition of a flat plate outboard of the triangle; it is further necessary to introduce a constant downwash in these regions to correspond to the angle of attack of the wing as a whole. This last must also be achieved without the introduction of additional downwash inboard of the panels. The net result is a change in lift on the portion of the original triangular wing within the Mach cone from the apex of each panel, which, together with the lift on the panels themselves, is to be calculated.



Sketch (a)

Notation

The symbols used in this report are defined in Appendix A. In addition to the Cartesian coordinate system (fig. 2) with origin at the apex of the wing, x axis positive downstream and z axis positive upward, a conical coordinate system in which the location of the origin is arbitrary will be used. Observed in the xy plane, the characteristic variable of such a system is the inclination of the line from the chosen origin x_i, y_i through the variable point x, y , the reference being the free-stream direction. For supersonic wing theory, the ratio of this quantity to the tangent of the Mach angle $1/\sqrt{M^2 - 1}$ is most significant. The conical variable (see sketch (b)) will therefore be chosen as



Sketch (b)

$$t = \beta \frac{y - y_i}{x - x_i}; \quad \beta = \sqrt{M^2 - 1}$$

with subscripts to indicate the location of the origin. For brevity, a line making the angle $\tan^{-1} t/\beta$ with the stream will frequently be referred to as "the ray t ." The lines $t = \pm 1$ are Mach lines, regardless of the origin.

In keeping with the foregoing coordinate system, the sweepback of the leading edge of the wing is expressed in terms of similar parameters:

$m_1 = \beta$ times the tangent of the semiapex angle of the wing, or the cotangent of the angle of sweep of the inner portion of the leading edge

$m_2 = \beta$ times the cotangent of the angle of sweep of the outer portion

The linear dimensions of the wings are defined in figure 2 and Appendix A.

Boundary Conditions for Elementary Solutions

The upwash field of the inside triangle can be written from reference 8, in terms of the conical variable $t_0 = \beta y/x$ (see fig. 3 and

Appendix A) as follows:

$$w_{\Delta}(t_0) = \frac{u_0}{m_1} \left[t_0 \sqrt{\frac{1-t_0^2}{t_0^2-m_1^2}} - E(\varphi, \sqrt{1-m_1^2}) \right]; \quad m_1 \leq |t_0| \leq 1 \quad (1)$$

where E is the elliptic integral of the second kind, with the argument

$$\varphi = \sin^{-1} \sqrt{\frac{1-t_0^2}{t_0^2-m_1^2}} \quad (2)$$

and u has the value

$$u_0 = \frac{m_1 V \alpha}{\beta E(\sqrt{1-m_1^2})} \quad (3)$$

The solution required to cancel this field is constructed by the superposition of a family of solutions with parameter t_0 , each solution having the following properties:

1. In the infinite sector between any ray $\beta y = t_0 x$ and the outer segment of the leading edge (hatched portion, fig. 4), the vertical velocity is constant.
2. Between the ray $\beta y = t_0 x$ and the Mach line crossing the wing from the intersection x_1, y_1 of the ray with the leading edge, the vertical velocity is zero. (It is assumed for the moment that the Mach line does not cross the leading edge of the opposite panel.)
3. Along the Mach line just described, all the velocity components of the cancellation field vanish.
4. Ahead of the leading edge (on the right, in fig. 4) the streamwise component of the perturbation velocity is zero.

The foregoing conditions define a conical flow field (ref. 4), that is, one in which the velocity components are constant along any ray from the origin or apex - in this case the point x_1, y_1 . The solution is therefore expressible as a function of the single variable

$$t_1 = \beta \frac{y - y_1}{x - x_1} \quad (4)$$

the ratio of the slope of a ray of the field to the inclination of the Mach lines.

The conditions specified are the same as for the flow field of a deflected, triangular leading-edge flap, and the required solutions have been given in that connection in reference 5. In the sections to follow, these solutions will be used to build up the required wing plan forms by the method of superposition, and the resulting lift and drag will be calculated. Because of differences in detail between the calculation of the lifting pressure at any point and of the integrated lift and drag, the remainder of the analysis will be presented with specific application to each of these problems.

LIFT DISTRIBUTION

Suppose the incremental lifting pressure coefficient associated with each elementary solution is

$$\Delta C_p(x, y, t_0) = -\frac{4}{V} \frac{w}{\pi} W(t_0) P(t_0, t_1) \quad (5)$$

in which W is the constant vertical velocity on the sector and V the stream velocity. Then the total increase in local lift at a point x, y due to canceling the upwash on one side of the wing is

$$\frac{8}{\pi} \left[\frac{w_{\Delta}(m_1)}{V} P(m_1, t_m) + \frac{1}{V} \int_{m_1}^{\tau_0(x, y)} \frac{dw_{\Delta}(t_0)}{dt_0} P(t_0, t_1) dt_0 \right] \quad (6)$$

where t_m is the value of t_1 when $t_0 = m_1$, or

$$t_m = \beta \frac{y - s_1}{x - c_1} \quad (7)$$

and $\tau_0(x, y)$ is the value of t_0 such that

$$t_1(x, y, \tau_0) = -1$$

Since

$$x_1 = \frac{m_2 - m_1}{m_2 - t_0} c_1 \quad (8)$$

and

$$\beta y_1 = t_0 x_1 \quad (9)$$

setting t_1 (eq. (4)) equal to -1 gives

$$\tau_0(x, y) = \frac{m_2(x + \beta y) - (m_2 - m_1)c_1}{(x + \beta y) + (m_2 - m_1)c_1} \quad (10)$$

Also needed for equation (6) is the derivative of w_Δ ,

$$w'_\Delta(t_0) = -m_1 u_0 \frac{\sqrt{1-t_0^2}}{(t_0^2 - m_1^2)^{3/2}}$$

In addition to canceling the downwash, it is necessary to take into account the effect of the incidence α of the panel. This effect is obtained from equation (5) with $W = -\alpha V$ and $t_0 = m_1$, so that the total lifting pressure induced at a point x, y by the addition of the panels to the inner triangle is

$$\Delta C_p(x, y) = \frac{8}{\pi} \left\{ \left[\alpha + \frac{w_\Delta(m_1)}{V} \right] P(m_1, t_m) + \int_{m_1}^{t_0} \frac{w'_\Delta(t_0)}{V} P(t_0, t_1) dt_0 \right\} \quad (11)$$

If the point x, y is on the inside triangle, the foregoing lift is added to the lift associated with the original triangular-wing solution:

$$C_{p_\Delta}(x, y) = \frac{4m_1 u_0 x}{V \sqrt{m_1^2 x^2 - \beta^2 y^2}} \quad (12)$$

and, if it lies within the Mach cones from the apexes of both left- and right-hand outer panels, $\Delta C_p(x, -y)$ must also be added. For wing B, tip corrections will also be derived, so that, for a point near the center of the trailing edge, the complete expression for the pressure might be

$$C_p(x, y) = C_{p_\Delta}(x, y) + \Delta C_p(x, y) + \Delta C_p(x, -y) + (\Delta C_p)_{tip}(x, y) + (\Delta C_p)_{tip}(x, -y) \quad (13)$$

Elementary Solutions

At this point it becomes necessary to specify whether the sweep of the Mach lines is greater or less than the sweep of the outer segment of the leading edge, that is, whether m_2 is greater or less than one. For $m_2 < 1$, the solution satisfying the specified conditions is given by equation (6.6) of reference 5, from which is obtained

$$[\mathbb{P}(t_0, t_1)]_{m_2 < 1} = m_2 P_1(t_0, t_1) - t_0 P_2(t_0, t_1) \quad (14)$$

with

$$P_1(t_0, t_1) = \frac{1}{1 + m_2} \sqrt{\frac{(m_2 - t_0)(1 + t_1)}{(1 - t_0)(m_2 - t_1)}} \quad (15)$$

and

$$P_2(t_0, t_1) = \frac{1}{\sqrt{1 - t_0^2}} \log \frac{\sqrt{(1 + t_0)(m_2 - t_1)} + \sqrt{(1 + t_1)(m_2 - t_0)}}{\sqrt{(1 + m_2)|t_0 - t_1|}} \quad (16)$$

These functions and the resultant pressure are plotted against t_1 in figure 5 for typical values of t_0 and m_2 . Note that the pressure is infinite along the subsonic leading edge and also when $t_1 = t_0$, the hinge-line location in the equivalent control-surface problem.

For $m_2 > 1$, the solution is identical with that on a vertically symmetrical wedge, with the lower-surface values changed in sign. The flow over the wedge, which is required to have a constant vertical velocity in the region between the leading edge and the extension of the ray t_0 across the wing (sketch (c)), may be constructed by subtracting from the flow field of a wedge, bounded by the leading edge and a line in the downstream direction from x_1, y_1 , the velocities over a wedge of equal inclination, bounded by the ray t_0 and the line drawn downstream from x_1, y_1 . The two component solutions may be obtained from reference 5, or more readily, from reference 10. The combined solutions give a pressure proportional to

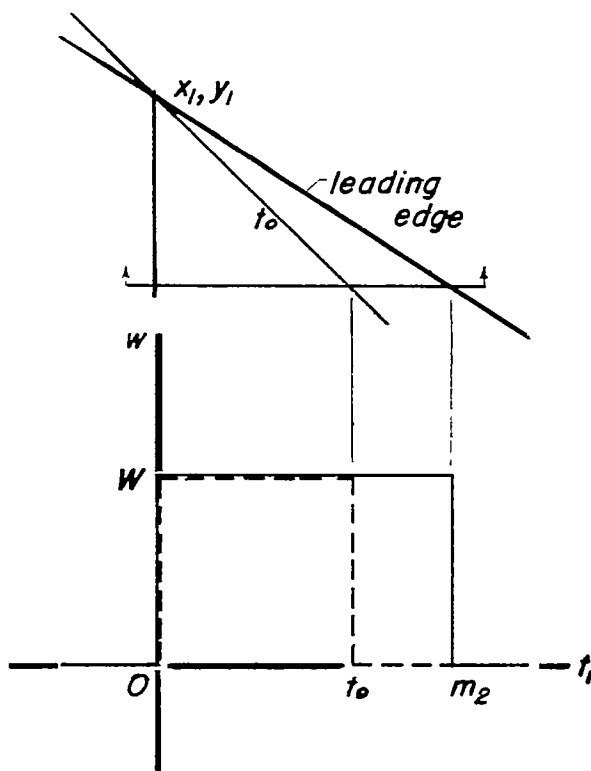
$$[\mathbb{P}(t_0, t_1)]_{m_2 > 1} =$$

$$m_2 Q_1(t_0, t_1) - t_0 Q_2(t_0, t_1) \quad (17)$$

with

$$Q_1(t_0, t_1) =$$

$$\frac{1}{\sqrt{m_2^2 - 1}} \cos^{-1} \sqrt{\frac{(1+m_2)(1-t_1)}{2(m_2-t_1)}} \quad (18)$$



Sketch (c)

and

$$Q_2(t_0, t_1) = \frac{1}{\sqrt{1 - t_0^2}} \log \frac{\sqrt{(1+t_0)(1-t_1)} + \sqrt{(1+t_1)(1-t_0)}}{\sqrt{2|t_0 - t_1|}} \quad (19)$$

These functions and the resultant pressure coefficient are plotted in figure 6.

Formulas and Lift Distribution - Leading Edge Entirely Subsonic

Formulas for ΔC_p . If $\mathbb{P}(t_0, t_1)$ (eq. (14)) is substituted in equation (11), the latter may be integrated (ref. 11) to give the following

result:

$$\Delta C_p(x, y) = -\frac{\delta u_o}{\pi V} \left\{ m_1 g(t, \tau_o) G_n - \frac{m_2(1+t)}{2m_1(1+m_2) g(t, \tau_o)} [2E(k) - k'^2 K(k)] \right\} \quad (20)$$

where

$$t = \frac{\beta y}{x}$$

$$g = \sqrt{\frac{(1+t)(\tau_o - t)}{(1+m_1)(\tau_o + m_1)}}$$

$$k = \sqrt{\frac{(1-m_1)(\tau_o - m_1)}{(1+m_1)(\tau_o + m_1)}}$$

$$k' = \sqrt{1 - k^2}$$

and

$$G_1 = K(k) \left[\frac{1}{m_1 - t} - \frac{Z(\theta_1, k)}{g \sqrt{t^2 - m_1^2}} \right]; \quad \theta_1 = \sin^{-1} \sqrt{\frac{(1+m_1)(t+m_1)}{(1-m_1)(t-m_1)}} \text{ for } t < -m_1$$

$$G_2 = \frac{-1}{1 - m_1} \left[K(k) - \frac{1+m_1}{2m_1} E(k) \right] \quad \text{for } t = -m_1$$

$$G_3 = -\frac{K(k)}{1+t} + \frac{\pi}{2} \frac{\Lambda_o(\theta_3, k)}{g \sqrt{m_1^2 - t^2}}; \quad \theta_3 = \sin^{-1} \sqrt{\frac{(1+m_1)(t+m_1)}{2m_1(1+t)}} \text{ for } -m_1 < t < m_1$$

$$G_4 = -K(k) \left[\frac{1}{t+m_1} - \frac{Z(\theta_4, k)}{g \sqrt{t^2 - m_1^2}} \right]; \quad \theta_4 = \sin^{-1} \sqrt{\frac{(t-m_1)(\tau_o + m_1)}{(t+m_1)(\tau_o - m_1)}} \text{ for } t > m_1$$

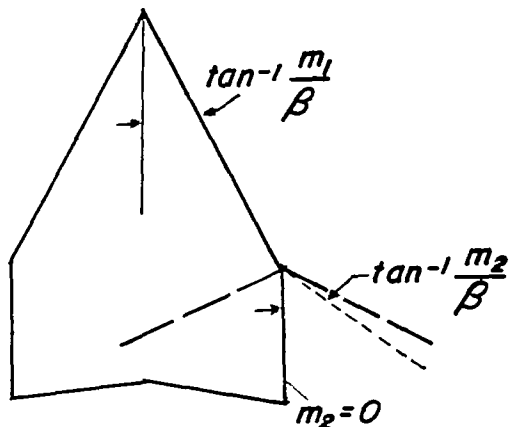
The elliptic functions $E(k)$, $K(k)$, $Z(\theta, k)$, and $\Lambda_o(\theta, k)$ are defined in Appendix A.

Along the inboard Mach line $y = y^*(x)$ from the apex c_1, s_1 of the panel, τ_o reduces to m_1 , and ΔC_p takes on the simple form

$$\Delta C_p[x, y^*(x)] = \frac{4u_\infty}{V} \frac{m_2 - m_1}{m_1(1+m_2)} \sqrt{\frac{\beta s_1}{2(1+m_1)(x - c_1)}} \quad (21)$$

Ahead of this line the effect of the panel is of course zero, so that the result is a finite step in the lift distribution. It is interesting to note that, with $m_2 = 0$, equation (21) gives the value of the decrement in lift along the corresponding Mach line from the outside corner formed by a streamwise tip on a simple sweptback wing (see sketch (d) and ref. 12).

Along the boundary between the outer panel and the inside triangle, t equals m_1 , G_s is infinite, and ΔC_p is double-valued. However, both the limit of $C_{p\Delta} + \Delta C_p$ as t approaches m_1 from below, and the limit of ΔC_p as t approaches m_1 from above (where $C_{p\Delta} = 0$) equal

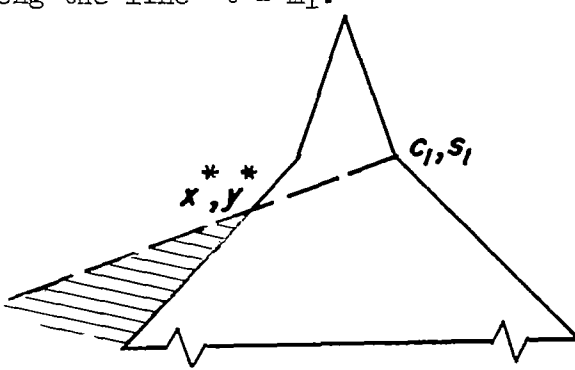


Sketch (d)

$$C_p\left(x, \frac{m_1 x}{\beta}\right) = -\frac{8u_\infty}{\pi V} \frac{m_1}{\sqrt{\tau_0^2 - m_1^2}} \left\{ K - \frac{\tau_0 + m_1}{2m_1} \left[E + \frac{m_2(l+m_1)}{m_1(l+m_2)} (2E - k^2 K) \right] \right\} \quad (22)$$

with the modulus of the elliptic integrals as defined for equation (20). It will be seen from the numerical results that the lift-distribution curve goes smoothly through this value, although the initial lift distribution $C_{p\Delta}$ went to infinity along the line $t = m_1$. Δ

If the inboard Mach line from c_1, s_1 intersects the opposite leading edge as in sketch (e), fictitious pressure differences will have been introduced, by the use of the conical fields, into the region ahead of the wing shown shaded in the sketch. Cancellation of these pressure differences is necessary in order to satisfy



Sketch (e)

the condition of continuity of pressure in the stream. Mathematically, this is a somewhat formidable task. As the pressures involved are actually not very great, it will usually be sufficient to perform only an approximate cancellation, as follows:

Assume ΔC_p to be constant and equal to $\Delta C_p(x^*, y^*)$ throughout the shaded region. Then it may be canceled, and the boundary conditions on the wing preserved, by a single conical field with its origin at x^*, y^* . In terms of the conical variable

$$t^* = \beta \frac{y - y^*}{x - x^*}$$

the boundary conditions on the solution are simply,

$$\frac{\frac{4u}{V}}{V} = \Delta C_p(x^*, y^*); \quad -1 \leq t^* \leq -m_2$$

$$w = 0; \quad -m_2 < t^* < +1$$

The required solution is obtained by a slight modification of equation (5.15'b) of reference 5:

$$\begin{aligned} (\Delta C_p)_{L.E.}(x, y) = & -\frac{1}{\pi} \Delta C_p(x^*, y^*) \left[\cos^{-1} \frac{2(m_2 + t^*) - (1 - m_2)(1 - t^*)}{(1 + m_2)(1 + t^*)} - \right. \\ & \left. \frac{2m_2 \sqrt{2(1 - m_2)}}{1 + m_2} \sqrt{\frac{1 - t^*}{m_2 + t^*}} \right] \end{aligned} \quad (23)$$

This term is to be added into equation (13).

Tip effect, wing B. - If the trailing edge of the wing is unswept, or is swept (either forward or back) but is everywhere supersonic, and if the tips are tapered to a point, the entire lift distribution due to angle of attack is given by the foregoing formulas. If the wing is not fully tapered, but has tips formed by any entirely subsonic curve, the lift on the portions of the wing included in the foremost Mach cones from the tip will be modified in a manner best calculated by the method of reference 6. If the tips are simply cut off parallel to the stream, the pertinent formula (17a) in reference 6 can be integrated after the

insertion of ΔC_p from equation (20)² to give

$$\begin{aligned} (\Delta C_p)_{tip}(x,y) = & \frac{-8m_1 u_o}{\pi V} \sqrt{\frac{(1+t)(\tau_1-t)}{(1+m_1)(\tau_o+m_1)}} \left\{ G_4(\tau_1) \sqrt{\frac{\tau_o+m_1}{\tau_1+m_1}} - G_4(\tau_o) \sqrt{\frac{\tau_o-t}{\tau_1-t}} + \right. \\ & \left. \frac{m_2(1+t)(t+m_1)}{2m_1^2(1+m_2)g^2(t,\tau_o)} \sqrt{\frac{\tau_o-t}{\tau_1-t}} \left[2E(k) - k'^2 K(k) \right] \right\} \quad (24) \end{aligned}$$

in which $G_4(\tau_1)$ is obtained by replacing τ_o by

$$\tau_1 = \frac{\beta s}{x - \beta(s-y)} \quad (25)$$

everywhere in G_4 , and k has the same value otherwise as in equation (20). Along the Mach line from the tip, τ_1 equals τ_o and $(\Delta C_p)_{tip}$ reduces to

$$(\Delta C_p)_{tip}\left(x, s - \frac{x-c_2}{\beta}\right) = - \frac{4m_2 u_o (1+t)(t+m_1)}{m_1 \pi V (1+m_2) g(t, \tau_o)} \left[2E(k) - k'^2 K(k) \right] \quad (26)$$

At the tip, the right-hand side of equation (24) becomes indeterminate, but reduces in the limit to $-\Delta C_p(x, s)$ as given by equation (20).

Numerical results. - The lift distribution at $M = \sqrt{2}$ was calculated for a wing with semiapex angle equal to $\tan^{-1} 0.375$ (that is, almost 70° sweep of the leading edge at the root) and 48° sweep of the leading edge of the outer panels. With $\beta = 1$, the sweep parameters were therefore $m_1 = 0.375$ and $m_2 = 0.9$. The linear dimensions of the wing and the Mach line pattern are shown in figure 7.

²It is assumed in this investigation that the region which has been referred to as the "inside triangle" is in fact a triangle, that is, that the inner portion of the leading edge, extended rearward, intersects the trailing edge rather than the tip. Formulas for the latter case can be derived by including C_p_Δ in the lift to be canceled at the tips.

The resulting lift distribution is shown (fig. 8) in spanwise sections, that is, for constant values of x . Ahead of and at the section $x = 4$, the lift coefficient is merely that (eq. (12)) on the triangular wing formed by the inner portion of the leading edge. At $x = 4.5$, the effect of the bend in the leading edge appears at $y = \pm 1$. The resulting step in the lift distribution mentioned earlier is seen to be quite pronounced. Between the Mach lines, the lift retains the relatively low value associated with the slender triangle.

At $x = 5.5$, the Mach lines intersect on the center line of the wing so that the steps do not appear individually. At $x = 8$, the Mach cones overlap and the effect of the outer panels is doubled in the center. The step at the Mach lines has fallen off considerably in magnitude.

The section at $x = 9$, otherwise similar to the preceding one, passes through the tip Mach cone. Again the discontinuity in lift appears at the Mach line. As in the case of the simple sweptback wing (ref. 12), the tip effect is so large as to destroy the major part of the lift within the Mach cone.

The span loadings obtained for this wing and for the type A wing derived from it by cutting off the rearmost portion ($x > 8$) are shown in figure 9. Also shown is the elliptical span loading of a triangular wing. In the case of the type B wing, the tip effect appears as a discontinuity in the slope of the span load curve. The bend in the leading edge does not, however, cause any abrupt change in the shape of the loading, as far as can be seen.

Aerodynamic center. - The pressure distributions of figure 8 were used to calculate the aerodynamic-center locations for the same wings for which the span loadings were calculated. The aerodynamic-center location was also determined at a Mach number of 1.2 and, using slender-wing theory (ref. 13), at $M = 1.0$. This last result is the same for both plan forms since, according to slender-wing theory, the non-expanding part of the wing is also nonlifting.

The lengthwise distributions of load, from which the centers of pressure were calculated, are shown in figure 10. The same curves apply to both wings up to $x = 8$, where the type A wing ends.

The aerodynamic-center locations are shown in figure 11. The aerodynamic center of the type A wing remains essentially fixed at $x = 6.04$ or $0.755 c_0$ for all three Mach numbers and thus lies considerably behind the center of area of the wing, which is at $x = 0.710 c_0$. The aerodynamic center of the blunt-tipped wing shifts from $x = 6.04$ or $0.604 c_0$ at $M = 1$ to $0.682 c_0$ for $M = 1.2$ and 1.4 , but still lies ahead of the center of area at $0.696 c_0$. These results may be compared with the triangular wing, for which the aerodynamic center, according

to linear theory, coincides with the center of area at 0.667 c_0 throughout the supersonic speed range.

Lift Distribution - Leading Edge of Outer Panel Supersonic

Formulas for ΔC_p . - The substitution of the elementary solution (eq. (17)) for $m_2 > 1$ in the integrals for ΔC_p (eq. (11)) results in hyperelliptic integrals which cannot be evaluated in terms of tabulated functions, except for the special cases $y = y^*(x)$ (the inboard Mach line from c_1, s_1) and points along the leading edge. Along the inboard Mach line, the result is

$$\Delta C_p(x, y^*) = \frac{2u_0}{m_1 V} \sqrt{\frac{(1 - m_1)(m_2 - m_1) \beta s_1}{(1 + m_1)(1 + m_2)(x - c_1)}} \quad (27)$$

Along the supersonic leading edge, the pressure is finite, having the value

$$(C_p)_{L.E.} = \frac{4m_2}{\sqrt{m_2^2 - 1}} \left[\alpha + \frac{w_\Delta(t)}{V} \right] \quad (28)$$

This latter is the two-dimensional value of the pressure coefficient, with the angle of attack increased by the local angle of upwash of the streamlines due to the projecting triangular region at the root.

Along the outer Mach line from the bend in the leading edge, the pressure is theoretically infinite, since the pressure for the elementary solution (eq. (17)) does not vanish along $t_1 = 1$ for the supersonic leading edge, and the magnitude w is infinite at $t_0 = m_1$. The resulting infinity is of power $1/2$, as was previously found by Morikawa (ref. 3) for the special case of a concave 90° corner.

The pressure on the wing elsewhere than along the lines just discussed must be found by numerical integration of equation (11). Since, with $m_2 > 1$, $P(t_0, t_1)$ is constant when t_1 is greater than 1 (fig. 6), equation (11) may be written, for points ahead of the Mach line from the bend in the leading edge,

$$\Delta C_p(x, y) = \frac{4m_2}{\sqrt{m_2^2 - 1}} \left[\alpha + \frac{w_\Delta(\tau_2)}{V} \right] + \frac{8}{\pi} \int_{\tau_2}^{t_0} \frac{w_\Delta'(t_0)}{V} P(t_0, t_1) dt_0 \quad (29)$$

in which

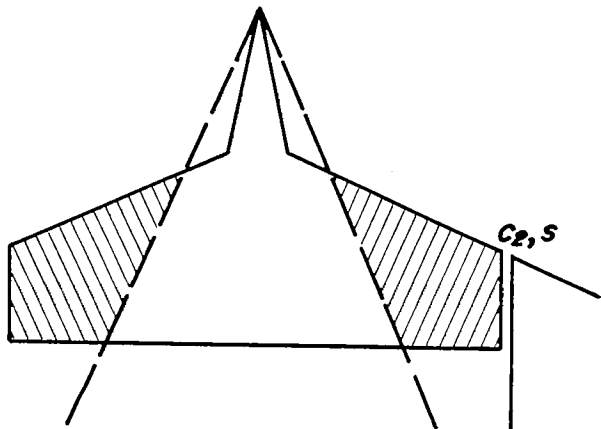
$$\tau_2 = \frac{(m_2 - m_1)c_1 - m_2(x - \beta y)}{(m_2 - m_1)c_1 - (x - \beta y)} \quad (30)$$

is the value of t_0 such that $t_1(x, y, \tau_2) = 1$.

If the point x, y is behind the Mach line, so that τ_2 is less than m_1 , the presence of the singularity in w_Δ' at $t_0 = m_1$ makes it advisable first to integrate equation (11) by parts, obtaining

$$\Delta C_p(x, y) = \frac{8}{\pi} \left[\alpha P(m_1, t_m) + \int_0^{P(m_1)} \frac{w_\Delta(t_0)}{v} dP(t_0, t_1) \right] \quad (31)$$

Tip effect. - If the Mach number, or aspect ratio, or both, are so large that the Mach lines from the apex of the wing intersect the trailing edge, as in sketch (f), the pressure coefficient in the shaded region is constant at the two-dimensional value



Sketch (f)

$$C_p = \frac{4m_2\alpha}{\sqrt{m_2^2 - 1}} \quad (32)$$

Then the tip effect can be found as the result of the superposition of a single conical flow field to cancel that pressure in the region indicated outboard of the wing tip in the sketch. The induced decrement in lift will be, from reference 5,

$$(\Delta C_p)_{tip}(x, y) = \frac{-4m_2\alpha}{\pi\sqrt{m_2^2 - 1}} \cos^{-1} \frac{m_2 + t_s + 2m_2t_s}{t_s - m_2} \quad (33)$$

with

$$t_s = \beta \frac{y - s}{x - c_2} \quad (34)$$

If a part of the tip section lies within the upwash field of the forward part of the wing, the effect on the lift distribution may again be calculated by Mirels' method. Inserting equations (29) and (31) in

equation (17a) of reference 6 and inverting the order of integration yield the following expressions for the tip-induced decrement to the pressure coefficient:

For points in region ABDE (see sketch (g))

$$\begin{aligned}
 (\Delta C_p)_{\text{tip}}(x, y) = & \frac{-8m_2}{\pi\sqrt{m_2^2-1}} \left\{ \left[\alpha + \frac{w_\Delta(\tau_s)}{V} \right] \tan^{-1} \sqrt{\frac{\xi-\eta_1}{\eta-\xi}} + \frac{1}{V} \int_{\tau_s}^{\tau_o} w_\Delta'(t_o) H(t_o) dt_o \right\} + \\
 & \frac{4m_1 u_o}{\pi V} \left[\frac{1}{\sqrt{\tau_s^2 - m_1^2}} \log \frac{\sqrt{(\tau_1-t)(1+\tau_s)} + \sqrt{(1+t)(\tau_1-\tau_s)}}{|\sqrt{(\tau_1-t)(1+\tau_s)} - \sqrt{(1+t)(\tau_1-\tau_s)}|} + \right. \\
 & \left. \sqrt{(1+t)(\tau_1-t)} \int_{\tau_s}^{\tau_1} \frac{dt_o}{(t-t_o)\sqrt{(t_o^2-m_1^2)(1+t_o)(\tau_1-t_o)}} \right] \quad (35a)
 \end{aligned}$$

with

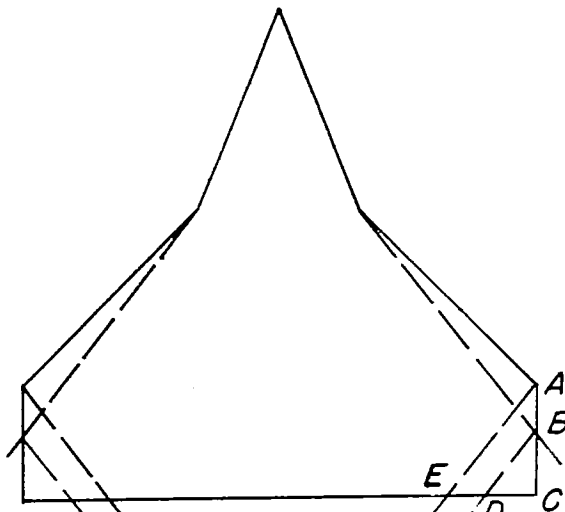
$$\xi = (x - c_2) - \beta(s - y)$$

$$\eta = (x - c_2) + \beta(s - y)$$

$$\eta_1 = -\frac{m_2 - 1}{m_2 + 1} \xi$$

$$\tau_s = \frac{(m_2-1)\beta s - m_2 \xi}{(m_2-1)c_2 - \xi}$$

$$H(t_o) = \tan^{-1} \sqrt{\frac{h(t_o) - \eta_1}{\eta - h(t_o)}} -$$



Sketch (g)

$$\frac{t_o}{2m_2 \sqrt{\frac{m_2^2-1}{1-t_o^2}}} \log \frac{\sqrt{(m_2-1)(1+t_o)} \sqrt{\eta-h(t_o)} + \sqrt{(m_2+1)(1-t_o)} \sqrt{h(t_o)-\eta_1}}{|\sqrt{(m_2-1)(1+t_o)} \sqrt{\eta-h(t_o)} - \sqrt{(m_2+1)(1-t_o)} \sqrt{h(t_o)-\eta_1}|}$$

$$h(t_o) = (m_2-1) \frac{\beta s - c_2 t_o}{m_2 - t_o}$$

For points in region BDC,

$$(\Delta C_p)_{tip}(x,y) = -\frac{8}{\pi} \left\{ \frac{m_2}{\sqrt{m_2^2 - 1}} \left[\alpha H(m_1) + \frac{1}{V} \int_0^{H(m_1)} w_\Delta(t_0) dH(t_0) \right] + \frac{m_1 u_0}{V} \sqrt{\frac{(1+t)(\tau_1-t)}{(1+m_1)(\tau_1+m_1)}} G_4(\tau_1) \right\} \quad (35b)$$

(See eqs. (20) and (24).)

Numerical results. - The lift distribution has been calculated for two spanwise sections of the previously considered wing, with 70° and 48° of sweep, at a Mach number of 1.667, so that $m_1 = 0.5$ and $m_2 = 1.2$. The Mach line pattern and the resulting lift distributions at $x = 5$ and $x = 10$ are presented in figure 12.

LIFT AND DRAG

Method of Calculating Total Lift

In applying the conical-flows method, the simplest procedure for calculating the lift is to determine the lift due to each conical field separately by integrating the expression for the pressure with respect to the conical variable of that field. Thus the lift on the inside triangle is found first, neglecting interference effects from the panels. The result may be written

$$\frac{L_\Delta}{q} = 2\pi \frac{m_1 u_0}{\beta V} c_0^2 \quad (36)$$

(It is assumed, as before, that the leading edge of the triangle does not intersect the tip of the wing.)

An expression for the incremental lift due to each elementary cancellation field is derived by integrating equation (5) with respect to t_1 over the proper area, which varies with the constant of the field, t_0 . The results are then combined in precisely the same way, except for the limits of integration, as in obtaining the expression for C_p . Thus, if the integrated lift per elementary cancellation field is given by

$$\frac{\Delta L(t_0)}{q} = \frac{-4}{\pi} \frac{w(t_0)}{\beta v} \bar{L}(t_0) \quad (37)$$

the total lift on and due to the outer panels is given by

$$\frac{\Delta L}{q} = \frac{8}{\pi \beta} \left\{ \left[\alpha + \frac{w_{\Delta}(m_1)}{v} \right] \bar{L}(m_1) + \int_{m_1}^{T_0} \frac{w_{\Delta}'(t_0)}{v} \bar{L}(t_0) dt_0 \right\} \quad (38)$$

which corresponds to equation (11) for the incremental pressure. (A factor of 2 has been introduced to provide for both right- and left-hand panels.) The upper limit

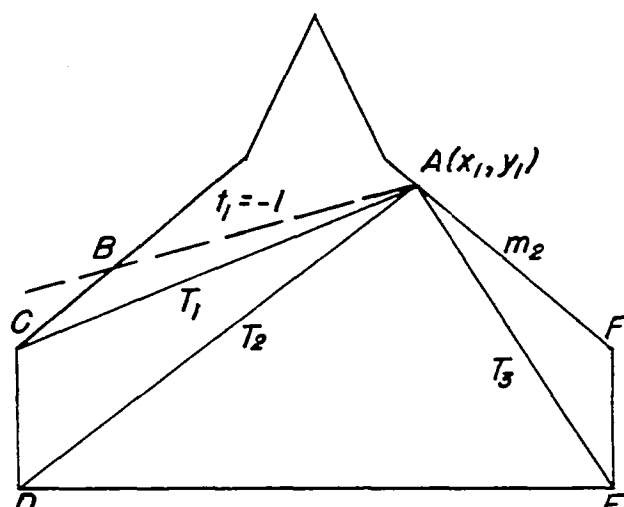
$$T_0 = \beta \frac{s}{c_2} \quad (39)$$

of the integral is the value of t_0 at the tip of the leading edge. If the tip is outside the Mach cone from the origin, the integral is of course taken only to $t_0 = 1$.

In the case of a wing of type B, it is necessary to take into account the presence of the tip, not only as it affects the area of integration, but also as it reduces the pressure at points within the tip Mach cone. The latter effect, previously calculated by Mirels' method, is more readily computed by the conical-flows method when the integrated lift is required.

If it is assumed as before that the line $t_0 = m_1$ does not intersect the tip, it is necessary to consider the tip-interference effect in the derivation of $\bar{L}(t_0)$ only. For each elementary upwash-cancellation field with apex at x_1, y_1 (fig. 13), the lifting pressure varies conically according to equation (14) or (17) between the Mach line $t_1 = -1$ and the leading edge $t_1 = m_2$, extended to infinity. The lift outboard of the tip must, however, be brought to zero. For a single conical field, this is readily accomplished by the superposition of other conical fields in a manner entirely analogous to the cancellation of upwash. The necessary formulas and the details of the procedure may be found in reference 12.

If the Mach line $t_1 = -1$ intersects the leading edge or the tip of the left-hand wing panel (as in sketch (h)), rather than the trailing edge,

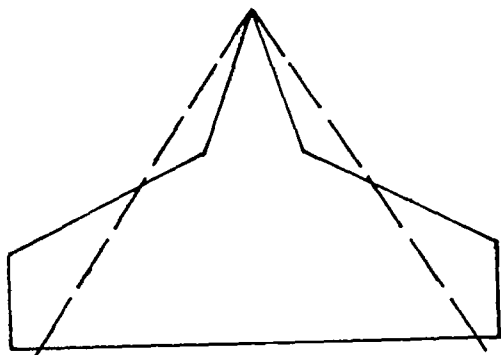


Sketch (h)

similar corrections to $L(t_0)$ should be made for the lift canceled at those boundaries. These effects are, however, mathematically very complex and in the calculations to be reported were incorporated, in an approximate way only, at the end of the computations. Cases in which these corrections might be any considerable fraction of the total lift were excluded from consideration.

When the integration of $\Delta C_p(t_0, t_1)$ is performed over the area ABCDEF of sketch (h), it is found to result in terms identical in value but opposite in sign to terms in the previously derived tip correction. It is most convenient, therefore, to use for $L(t_0)$ in equation (38) the value from the combined or net lift. The resulting formulas are listed for the various cases in Appendix B.

Unfortunately, in the general case, substitution of $L(t_0)$ in equation (38) results in incomplete elliptic integrals of the third kind, which are as yet untabulated and exceedingly tedious to compute. There is nothing to be gained, therefore, by performing the integration analytically, and the equation is left for numerical evaluation.



Sketch (i)

In the special case shown in sketch (i), in which the Mach number is so high that the entire tip is outside the Mach lines from the apex of the wing, the elliptic integrals become complete, and the resulting formula is readily computed with the aid of the tables of reference 11 or 14. In this case the lift-curve slope of the complete wing is as follows:

$$C_{L\alpha} = \frac{4}{\beta S} \left\{ \frac{m_2 - m_1}{m_2 + m_1} \frac{s_1^2}{E} \left[\frac{\pi}{2} (1 + \Lambda_0) \sqrt{\frac{m_2^2 - 1}{m_2^2 - m_1^2}} + \frac{1}{m_2} \left(\frac{m_2^2}{m_1^2} E - K \right) \right] + \right. \\ \left. m_2 c_0^2 - 2c_0 c_1 (m_2 - m_1) - m_2 (c_0 - c_2)^2 \sqrt{\frac{m_2}{m_2 - 1}} \right\} \quad (40)$$

where S is the wing area and Λ_0 , E , and K are the elliptic integrals (Appendix A) with modulus $\sqrt{1 - m_1^2}$ and, in Λ_0 , the argument

$$\phi = \sin^{-1} \frac{1}{m_2}$$

Method of Computing Drag

The drag on a flat-plate wing at an angle of attack is the difference between the rearward component of the normal-force vector and the thrust due to leading-edge suction. Using linear theory to evaluate the first of these forces, we write

$$D = \alpha L - T \quad (41)$$

The thrust T is calculated by integrating along the subsonic portion of the leading edge the streamwise component of the local suction force. If $x, y_1(x)$ are the coordinates of a point on the leading edge and m is the ratio of the inclination of the leading edge at that point to the tangent of the Mach angle, then, from reference 8, the contribution to the thrust at the point x, y_1 is given by

$$\frac{dT}{dx} = \frac{\rho\pi}{m} \sqrt{1-m^2} \left[\lim_{y \rightarrow y_1} u(x, y) \sqrt{\beta(y_1-y)} \right]^2 \quad (42)$$

where u is the streamwise component of the perturbation velocity.

Over the inside portion of the wings under consideration, $m = m_1$, $y_1 = \frac{m_1}{\beta} x$, and u , near the leading edge, has the value $\frac{m_1 u_0 x}{\sqrt{m_1^2 x^2 - \beta^2 y^2}}$ as in equation (12), from which is obtained

$$\frac{dT}{dx} = \frac{\rho\pi}{2} u_0^2 \sqrt{1-m_1^2} x; \quad x < c_1 \quad (43)$$

Then the total thrust over the inner portion of the leading edge is

$$2 \int_0^{c_1} \frac{dT}{dx} dx = \frac{\rho}{2} \pi u_0^2 c_1^2 \sqrt{1-m_1^2} \quad (44)$$

If m_2 is greater than 1, equation (44) gives the total thrust. If m_2 is less than 1, there is thrust along the outer portion of the wing as well. The velocity u in this region is found from equation (20). In equation (20), the term containing G_n remains finite as the leading edge is approached, so that it contributes nothing to the limit of the product in equation (42). The remaining term gives for the local thrust

$$\frac{dT}{dx} = \frac{m_2}{\pi} \rho u_0^2 \sqrt{\frac{1-m_2}{1+m_2}} x F_T(t) \quad (45)$$

where

$$F_T(t) = \frac{(1+m_1)(t+m_1)}{m_1^2} \left[2E(k) - k'^2 K(k) \right]^2 \quad (46)$$

$$k = \sqrt{\frac{(1-m_1)(t-m_1)}{(1+m_1)(t+m_1)}}; \quad t = m_2 - (m_2 - m_1) \frac{c_1}{x}$$

While it is not feasible to integrate equation (45) analytically, it has been found possible to approximate the product $x F_T(t)$, within the accuracy of our computations, by a linear expression which, when integrated, gives

$$2 \int_{c_1}^{c_2} \frac{dT}{dx} dx \cong \frac{2m_2}{\pi} \rho u_0^2 \sqrt{\frac{1-m_2}{1+m_2}} (c_2 - c_1) \left[c_2 F_T(T_O) - \frac{1}{2} (c_1 + c_2) F_T(m_2) \right] \quad (47)$$

If a portion of the leading edge lies within the Mach cone from the bend in the opposite leading edge, as in sketch (e), there may be a considerable effect on the leading-edge thrust on that portion. Making use of the approximation of equation (23) to modify the strength of the leading-edge singularity in the pressure, retaining the linear approximation for $x F_T(t)$, and dropping the square of the small correction contributed by equation (23), result in an additional term in the thrust:

$$\begin{aligned} 2 \int_{x^*}^{c_2} \frac{d\Delta T}{dx} dx &\cong \\ \frac{2m_2}{\pi m_1} \rho u_0^2 \frac{m_2 - m_1}{\sqrt{2(1+m_1)}} \left(\frac{1-m_2}{1+m_2} \right)^{3/2} &\left\{ \left[\frac{F_T(T_O)}{F_T(m_2)} c_2 + (c_2 - x^*) \right] \sqrt{c_2(c_2 - x^*) F_T(T_O)} + \right. \\ \sqrt{F_T(m_2)} \left[\frac{F_T(T_O)}{F_T(m_2)} c_2 - (c_2 - x^*) \right]^2 \cosh^{-1} &\left. \sqrt{\frac{c_2 F_T(T_1)}{c_2 F_T(T_1) - (c_2 - x^*) F_T(m_2)}} \right\} \end{aligned} \quad (48)$$

The drag is then calculated by substituting in equation (41) the thrust given by equation (44) and, if applicable, equations (47) and (48).

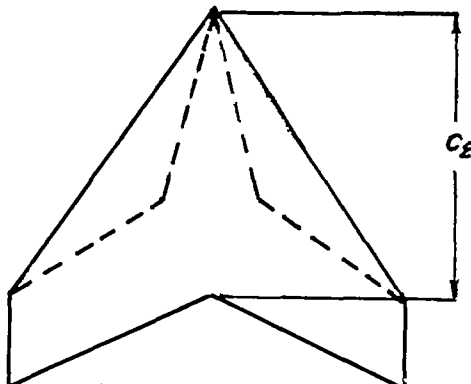
Numerical Results - Lift and Drag

The lift and the drag due to lift were calculated for a large number of wing plan forms, without, however, more than sampling the possible effects of the numerous parameters. The results are summarized in figures 14, 15, and 16.

In figure 14, the ratio of inner to outer slope of the leading edge, the ratio of c_1 to the root chord, and the ratio of s_1 to total semispan are fixed. Comparison is then made between the type B wing and a conventional sweptback wing of the same area, aspect ratio, and average sweep through a range of aspect ratios or, alternatively, through a range of Mach numbers, since any one curve can be interpreted as showing the effect of Mach number on a specific plan form.

Sketch (j) shows the method of deriving the conventional swept wing from the wing of type B. The tip chord was kept unchanged for the comparison because of the large loss in lift caused by the tip effect. The term "average sweep" is used in only a general sense, since no exact equivalence can be said to exist.

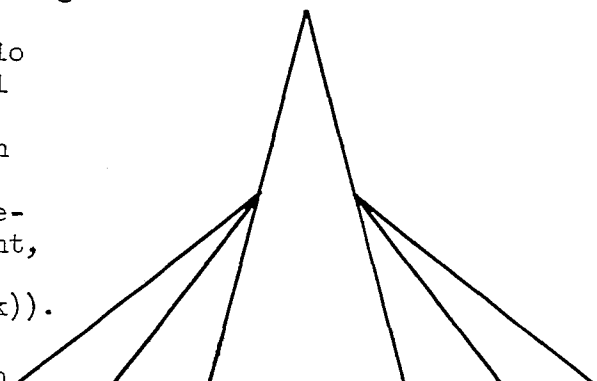
Comparison is also made with a type A wing having the same m_1/m_2 and s_1/s ratios and approximately the same c_1/c_0 ratio. A single calculation made with c_1/c_0 exactly equal to the value used for the type B wings showed this parameter to have little effect under the circumstances.



Sketch (j)

Curves showing the variation with aspect ratio of the lift and drag of rectangular and triangular wings are included for reference.

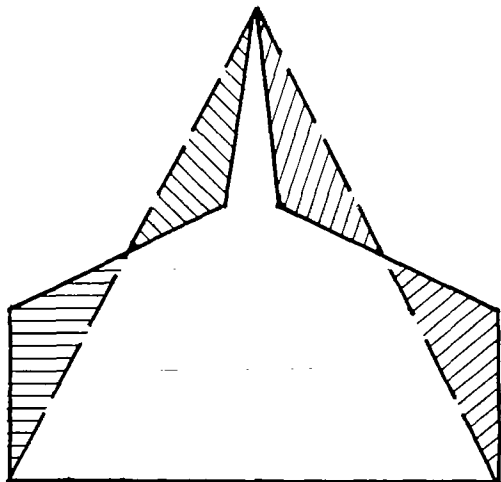
For figure 14, the aspect ratio was changed by the expansion of all the spanwise dimensions of a basic wing. In figure 15 the increase in aspect ratio is obtained by adding to a basic triangle triangular side-panels of increasing spanwise extent, starting at a fixed point back of the apex of the wing (see sketch (k)). Thus a family of cranked wings of type A is derived with fixed c_1/c_0 and m_1 , but increasing m_2 , area,



Sketch (k)

and aspect ratio. The resulting variations in lift and drag-rise factor are shown for two values of m_1 and two values of c_1/c_0 . It should be noted that, since m_1 is kept fixed, the variation shown does not correspond to the effect of Mach number change.

The curves for the sweptback wings in figures 14 and 15 all show a more or less abrupt break when the leading edge coincides with the Mach lines, followed by a levelling off of the curves at higher aspect ratios. In the cases of discontinuously swept wings, the breaks appear when $m_2 = 1$, since m_1 was kept less than 1 throughout the calculations. The effect of variations in the sweep angles of the leading edge is further shown in figure 16, where the aspect ratio is constant, and only the shape of the leading edge is varied. The cranked wings considered in this figure are all derived from an aspect ratio 2 triangle by increasing the sweep of the leading edge at the root and adding compensating area at the tips (see sketch (1)). The results are plotted against the ratio c_1/c_0 - the chordwise extent of the region of increased sweep - for selected values of m_1 , and cross-plotted for constant values of m_2 .



Sketch (1)

DISCUSSION OF RESULTS

The over-all characteristics of the cranked wings studied show no striking effects of the concentration of sweep near the root, at least as far as the lifting condition is concerned and omitting any consideration of the effect on the boundary-layer flow. The characteristics of the wings appear to be determined primarily by the sweep of the outer portion of the leading edge, the

increase in lift in these regions due to the more highly swept portions ahead being nullified by the decrease in lift in the center due to the small apex angle of the wing. In fact, the lift on the fully tapered (type A) wing is just about that on the triangular wing formed by the extension of the outer portions of the leading edge inward to the center line. Compared with triangular wings of the same aspect ratio, these wings show both lower values of the lift coefficient and higher values of the drag-rise factor. The calculations for the type B wings show a higher lift-curve slope than for conventional wings of the same average sweep and aspect ratio as long as the outer portions of the leading edge are subsonic, but also show higher drag due to lift.

The use of a cranked leading edge has a marked effect on the distribution of lift. Comparison with the triangular wing having the same leading-edge sweep as that of the outer panels shows the pressure at

the rear to be essentially unchanged by the addition of the forward peak within the overlapped Mach cones from the bend in the leading edge, but to be reduced abruptly ahead of this region, approximately in proportion to the apex angle of the wing. The lift near the outer portion of the leading edge, on the other hand, is increased by the upwash from the forward area and, if the outer portion of the leading edge is supersonic, the theory indicates infinite pressure along the outgoing Mach line from the bend. Somewhat the same effects may be anticipated behind the juncture of wing and fuselage in a complete airplane configuration.

The center of pressure of the cranked wing lies behind the center of area if the tips are tapered to a point, but may lie ahead of the center of area if the tip chord is a considerable fraction of the root chord, because of the large loss of lift inside the tip Mach cone. In the range of Mach numbers investigated there was no movement of the aerodynamic center with change of speed.

Any general conclusions regarding the value of the plan forms studied would have to take into account the possibilities offered in the way of a redistribution of thickness and the effect of the variation in sweep on the boundary-layer flow. The similarity of some of the plan forms to those of wing-body combinations suggests also that comparisons should really be made with such complete configurations, taking into consideration questions of total drag, weight and useful volume. These questions, though of prime importance, are beyond the scope of this report.

Ames Aeronautical Laboratory
National Advisory Committee for Aeronautics
Moffett Field, Calif., March 18, 1953.

APPENDIX A

SYMBOLS

General

V	free-stream velocity
M	free-stream Mach number
ρ	density of air
α	angle of attack, radians
β	$\sqrt{M^2 - 1}$
u	horizontal perturbation velocity, positive downstream
w	vertical perturbation velocity, positive upward
u_0	streamwise component of the perturbation velocity along the center line of a flat triangle at an angle of attack, with semiapex angle less than Mach angle (eq. (3))
w_Δ	upwash of a flat triangle at an angle of attack α , with semiapex angle less than Mach angle (eq. (1))
L	lift
D	drag
T	thrust
C_p	coefficient of lifting pressure, $\frac{4u}{V}$
$C_{p\Delta}$	coefficient of lifting pressure on flat triangle at angle of attack α , with semiapex angle less than Mach angle (eq. (12))
ΔC_p	coefficient of lifting pressure added by presence of each outer panel
$(\Delta C_p)_{tip}$	coefficient of lifting pressure added by presence of tip

Wing Dimensions

S	wing area
s	wing semispan

c_0	root chord (fig. 2)
c_1	streamwise distance from apex of wing to bend in leading edge (fig. 2)
c_2	streamwise distance from apex of wing to tip of leading edge (fig. 2)
s_1	spanwise distance from wing center line to bend in leading edge
m_1	β times the slope of the inner segment of the leading edge
m_2	β times the slope of the outer segment of the leading edge

Coordinates

x, y	Cartesian coordinates, positive downstream and to the right of the flight direction, respectively
x_1, y_1	coordinates of point on the leading edge (eqs. (8) and (9))
x_2, s	coordinates of intersection of ray from x_1, y_1 with tip chord
$y^*(x)$	y expressed as a function of x for points along the inboard Mach line from the point c_1, s_1
x^*, y^*	coordinates of intersection of inboard Mach line from c_1, s_1 with the leading edge of the left-hand panel
t_0	β times the slope of a line from the apex of the wing
t_1	β times the slope of a line from x_1, y_1 to the point at which the pressure is being calculated (eq. (4))
t	t_0 of the point at which the pressure is being calculated
$\tau_0, \tau_1, \tau_2, \tau_3$	limiting values of t_0 (τ_0 given by eq. (10), τ_1 by eq. (25), others defined where used)
t^*	β times the slope of a line from x^*, y^*
t_m	β times the slope of a line from c_1, s_1 (eq. (7))
t_s	β times the slope of a line from c_2, s (eq. (34))

T_0 β times the slope of the line joining the apex and the leading-edge tip (eq. (39))

T_1, T_2, T_3 β times the slope of the lines from x_1, y_1 to $(c_2, -s)$, $(c_0, -s)$, and (c_0, s) , respectively

Mathematical Symbols

\mathbb{P} function of t_1 proportional to lifting pressure in upwash-canceling solution (eqs. (14) and (17))

P_1, P_2 functions entering into \mathbb{P} for $m_2 < 1$ (eqs. (15) and (16))

Q_1, Q_2 functions entering into \mathbb{P} for $m_2 > 1$ (eqs. (18) and (19))

G_n, g functions entering into ΔC_p for $m_2 < 1$ (eq. (20))

L function of t_0 proportional to the total lift induced by an upwash-canceling solution

F_T function of t entering into the calculation of the leading-edge thrust (eq. (46))

k modulus of elliptic integrals, defined where used

k' complementary modulus ($\sqrt{1 - k^2}$)

ϕ, θ , or ψ argument of elliptic integrals, defined where used

$F(\phi, k)$ incomplete elliptic integral of the first kind of argument ϕ and modulus k

$E(\phi, k)$ incomplete elliptic integral of the second kind of argument ϕ and modulus k

$K, K(k)$ complete elliptic integral of the first kind; that is,

$$K = F\left(\frac{\pi}{2}, k\right)$$

$E, E(k)$ complete elliptic integral of the second kind; that is,

$$E = E\left(\frac{\pi}{2}, k\right)$$

Z Jacobian zeta function; $Z(\phi, k) = E(\phi, k) - \frac{E(k)}{K(k)} F(\phi, k)$
 $(KZ(\phi k)$ is tabulated in ref. 11.)

Λ_O function used in evaluating elliptic integral of third kind, circular case;

$$\Lambda_O(\phi, k) = \frac{2}{\pi} \left\{ K(k) E(\phi, k') - [K(k) - E(k)] F(\phi, k') \right\}$$

(tabulated in refs. 11 and 14)

APPENDIX B
FORMULAS FOR LIFT

For $m_2 < 1$,

$$\begin{aligned} \mathbb{L}(t_o) = & -2s^2 P_1(t_o, T_1) + \frac{m_2}{m_2+t_o} (s+c_2 t_o)^2 P_2(t_o, T_1) - \\ & y_1^2 \frac{m_2-t_o}{m_2+t_o} \sqrt{\frac{2(m_2-t_o)}{m_2(1-m_2)(1-t_o)}} \sinh^{-1} \sqrt{\frac{2m_2(1+T_1)}{(1+m_2)|m_2+T_1|}} + \\ & (c_o-x_1)^2 \left[(m_2-T_2)^2 P_1(t_o, T_2) - (t_o-T_2)^2 P_2(t_o, T_2) - \right. \\ & \left. \frac{(m_2-t_o)^{3/2}}{\sqrt{1-t_o}} \left(\sin^{-1} \sqrt{\frac{1+T_2}{1+m_2}} - \sin^{-1} \sqrt{\frac{T_2}{m_2}} \right) - \right. \\ & \left. \frac{(m_2-T_3)^2}{m_2} \sqrt{\frac{T_3(m_2-t_o)}{(1-t_o)m_2-T_3}}} + \frac{(t_o-T_3)^2}{\sqrt{t_o(1-t_o)}} \log \frac{\sqrt{t_o(m_2-T_3)} + \sqrt{T_3(m_2-t_o)}}{\sqrt{m_2 |t_o-T_3|}} \right] \end{aligned}$$

The terms in T_1 and T_2 vanish when T_1 and T_2 equal -1. If the Mach cone from x_1, y_1 does not include the far tip, T_1 and T_2 are less than -1 and the inapplicable terms are imaginary. For wings of type A, with zero tip chord, T_1 equals T_2 and T_3 equals m_2 , and the formula is accordingly simplified.

For $m_2 = 1$,

$$\begin{aligned} \mathbb{L}(t_o) = & (c_o-x_1)^2 \left[\frac{1-T_2}{2} \sqrt{1-T_2^2} - (t_o-T_2)^2 Q_2(t_o, T_2) - \right. \\ & (1-t_o) \left(\sin^{-1} \sqrt{\frac{1+T_2}{2}} - \sin^{-1} \sqrt{T_2} \right) - (1-T_3) \sqrt{T_3(1-T_3)} + \\ & \left. \frac{(t_o-T_3)^2}{\sqrt{t_o(1-t_o)}} \log \frac{\sqrt{t_o(1-T_3)} + \sqrt{T_3(1-t_o)}}{\sqrt{|t_o-T_3|}} \right] \end{aligned}$$

For $m_2 > 1$,

$$\begin{aligned} \mathbb{L}(t_o) = & (c_o - c_1)^2 \left[(m_2 - T_2)^2 Q_1(t_o, T_2) - (t_o - T_2)^2 Q_2(t_o, T_2) - \right. \\ & (m_2 - t_o) \left(\sin^{-1} \sqrt{\frac{1+T_2}{2}} - \sin^{-1} \sqrt{T_3} \right) - \frac{(m_2 - T_3)^2}{\sqrt{m_2(m_2 - 1)}} \cos^{-1} \sqrt{\frac{m_2(1-T_3)}{m_2 - T_3}} + \\ & \left. \frac{(t_o - T_3)^2}{\sqrt{t_o(1-t_o)}} \log \frac{\sqrt{t_o(1-T_3)} + \sqrt{T_3(1-t_o)}}{\sqrt{|t_o - T_3|}} \right] \end{aligned}$$

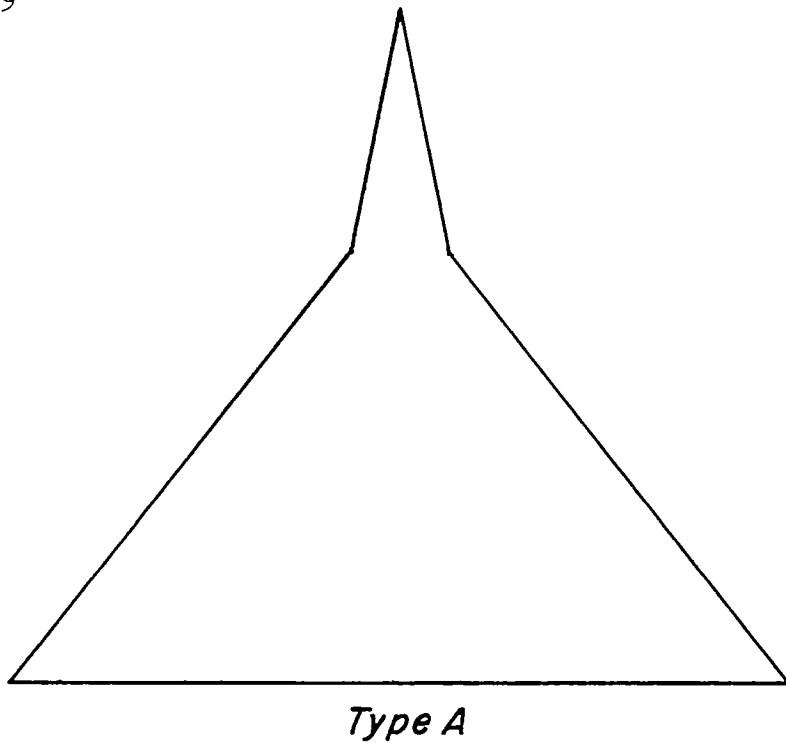
For $m_2 = \infty$,

$$\begin{aligned} \mathbb{L}(t_o) = & (c_o - c_1)^2 \left[(t_o - 2T_2) \sin^{-1} \sqrt{\frac{1+T_2}{2}} - (t_o - T_2)^2 Q_2(t_o, T_2) + \right. \\ & \frac{1}{2} \left(\sqrt{T_3(1-T_3)} - \sqrt{1-T_2^2} \right) + \left(2T_3 - t_o - \frac{1}{2} \right) \sin^{-1} T_3 + \\ & \left. \frac{(t_o - T_3)^2}{\sqrt{t_o(1-t_o)}} \log \frac{\sqrt{t_o(1-T_3)} + \sqrt{T_3(1-t_o)}}{\sqrt{|t_o - T_3|}} \right] \end{aligned}$$

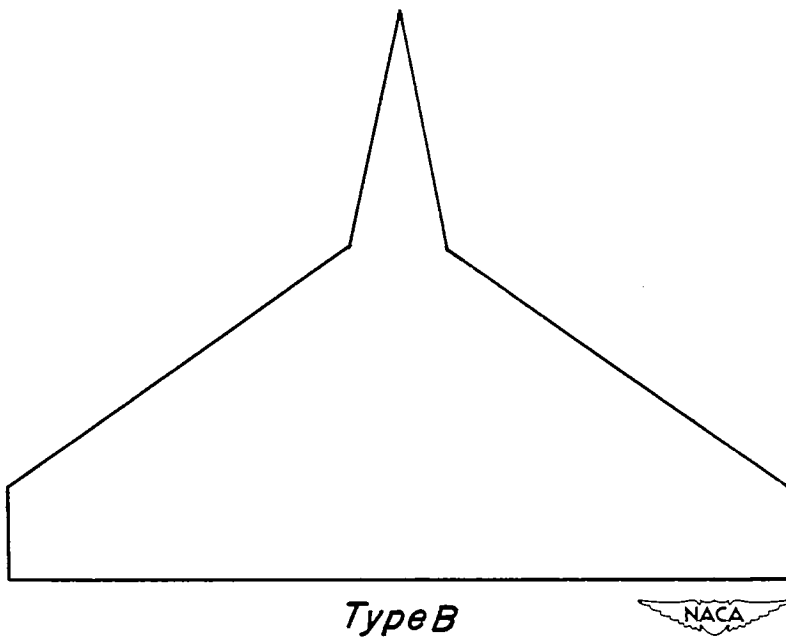
REFERENCES

1. Krüger, W.: Six-Component Measurements on a Cranked Swept-Back Wing for AR 23 $\frac{1}{4}$. Ministry of Aircraft Production, Völkenröde. British Rep. and Trans. No. 816, 1947.
2. Luckert, H. J.: High-Speed Investigations on Various Wing Forms and Wing Sections for the Development of the Arado 23 $\frac{1}{4}$ Wing. Ministry of Aircraft Production, Völkenröde. British Rep. and Trans. No. 279, 1947.
3. Morikawa, George K.: The Wing-Body Problem for Linearized Supersonic Flow. Progress Rep. No. 4-116, Jet Propulsion Lab., C.I.T., Dec. 19, 1949.
4. Busemann, A.: Infinitesimal Conical Supersonic Flow. NACA TM 1100, 1947.
5. Lagerstrom, P. A.: Linearized Supersonic Theory of Conical Wings. NACA TN 1685, 1948.
6. Mirels, Harold: A Lift-Cancellation Technique in Linearized Supersonic-Wing Theory. NACA Rep. 1004, 1951.
7. Stewart, H. J.: The Lift of a Delta Wing at Supersonic Speeds. Quart. of Appl. Math., vol. IV, no. 3, Oct., 1946.
8. Hayes, Wallace D.: Linearized Supersonic Flow. North American Aviation Inc., Rep. AL-222, June 18, 1947.
9. Germain, Paul: The General Theory of Conical Motions and Its Application to Supersonic Aerodynamics. ONERA Pub. No. 34, 1949.
10. Jones, Robert T.: Thin Oblique Airfoils at Supersonic Speed. NACA Rep. 851, 1946.
11. Byrd, Paul F., and Friedman, Morris D.: Handbook of Elliptic Integrals for Engineers and Physicists. Vol. LXVII, Grundl. d. math. Wiss., Springer-Verlag (Heidelberg).
12. Cohen, Doris: Formulas for the Supersonic Loading, Lift and Drag of Flat Swept-Back Wings with Leading Edges Behind the Mach Lines. NACA Rep. 1050, 1951.
13. Jones, Robert T.: Properties of Low-Aspect-Ratio Pointed Wings at Speeds Below and Above the Speed of Sound. NACA Rep. 835, 1946.

14. Heumann, Carl: Tables of Complete Elliptic Integrals. Jour. of Math. and Phys., vol. 19-20, 1940-41, pp. 127-206.



Type A



Type B



Figure 1.— Plan forms typical of the two classes considered.

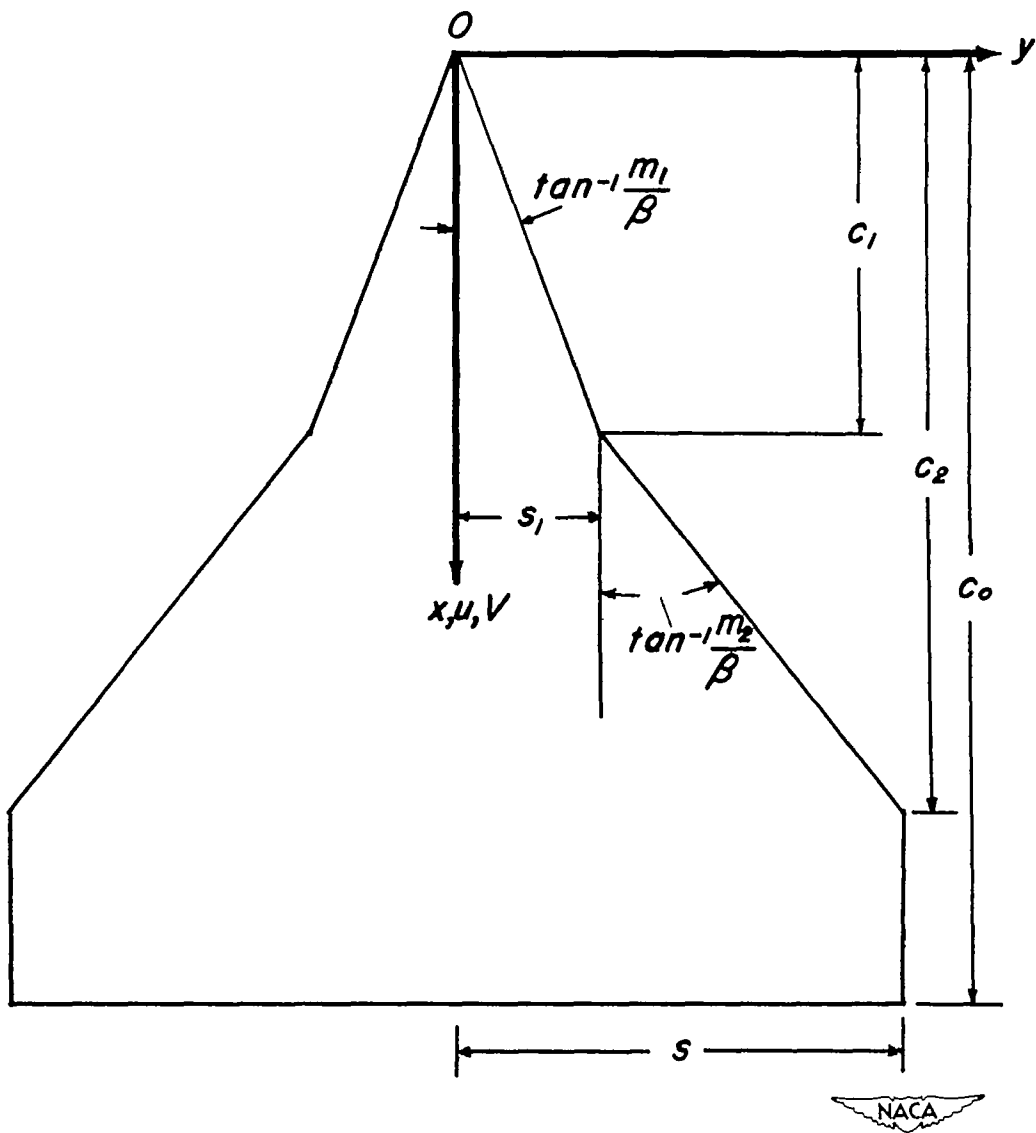


Figure 2.— Cartesian coordinates and plan-form parameters.

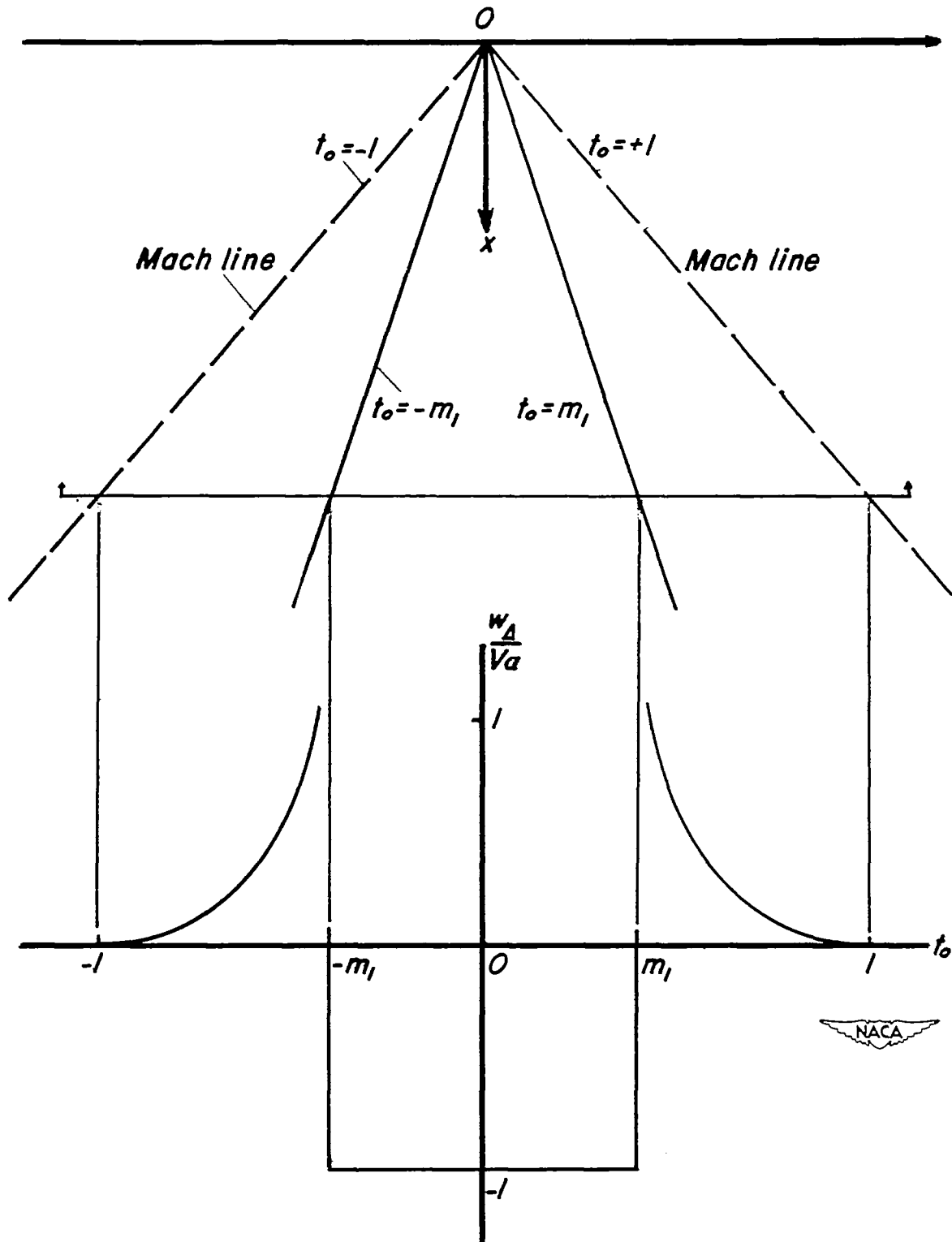


Figure 3.— Upwash field for flat triangular wing at an angle of attack and in moderately supersonic flight (Mach lines ahead of leading edge).

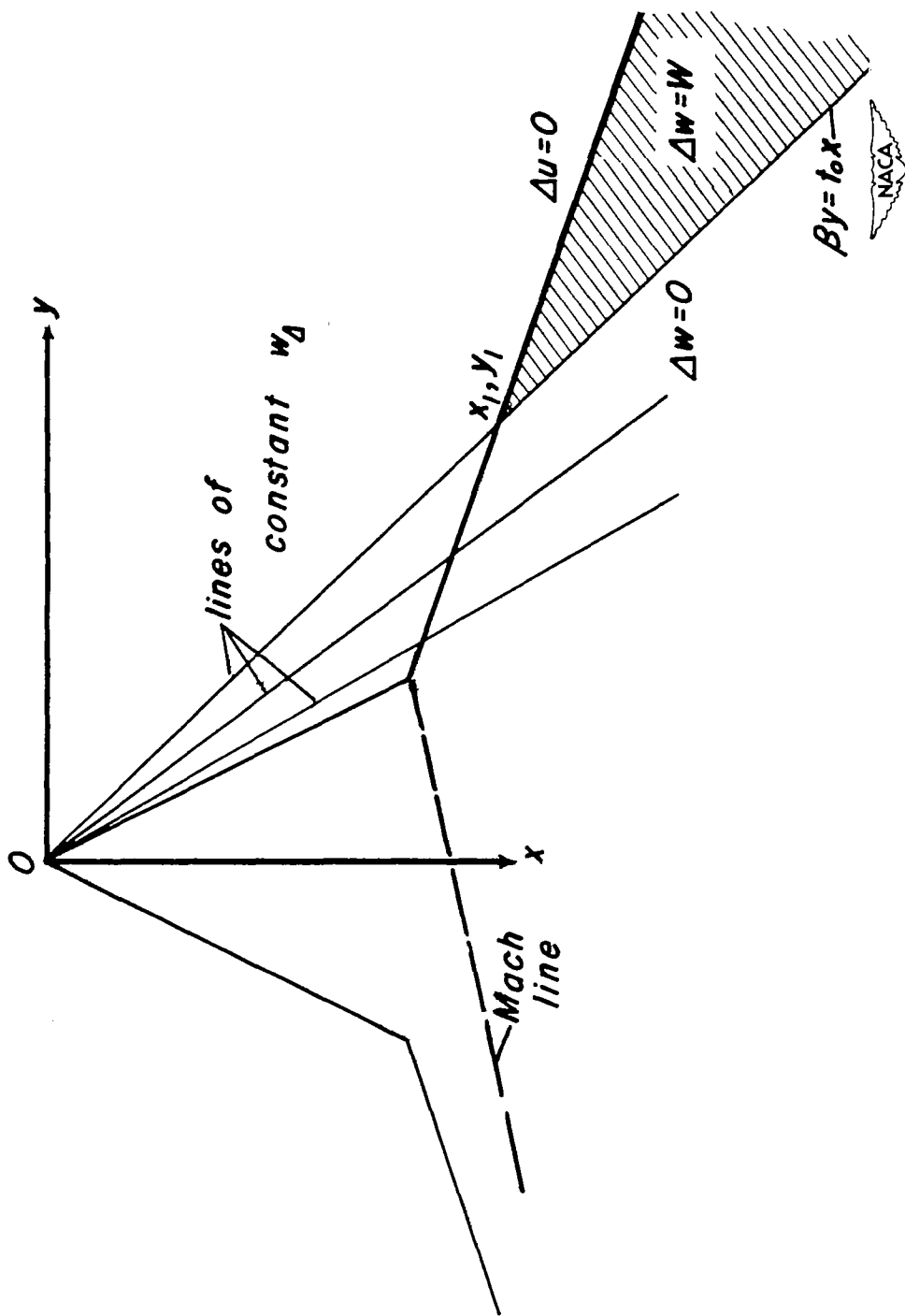


Figure 4.— Boundary conditions for elementary solution.

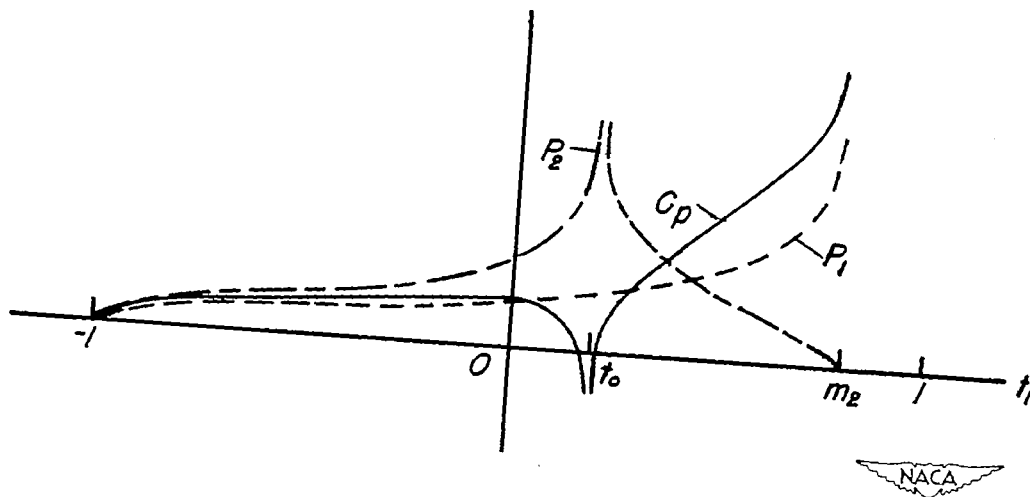


Figure 5.- Functions P_1 and P_2 and lift distribution of elementary solution, $m_2 < 1$.

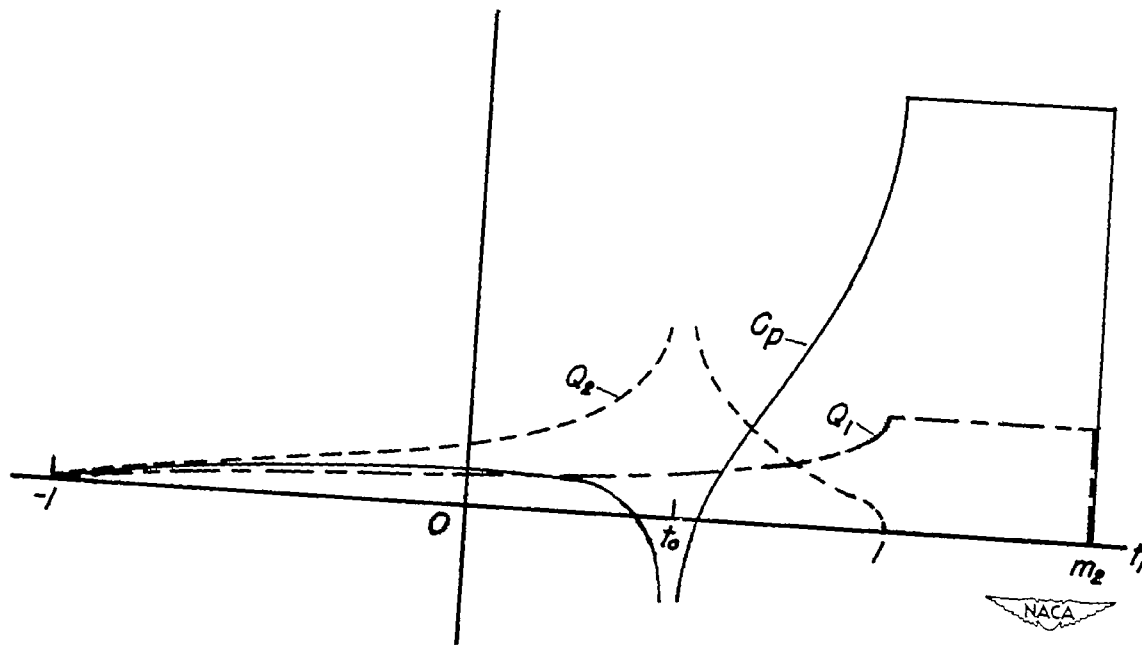


Figure 6.- Functions Q_1 and Q_2 and lift distribution of elementary solution, $m_2 > 1$.

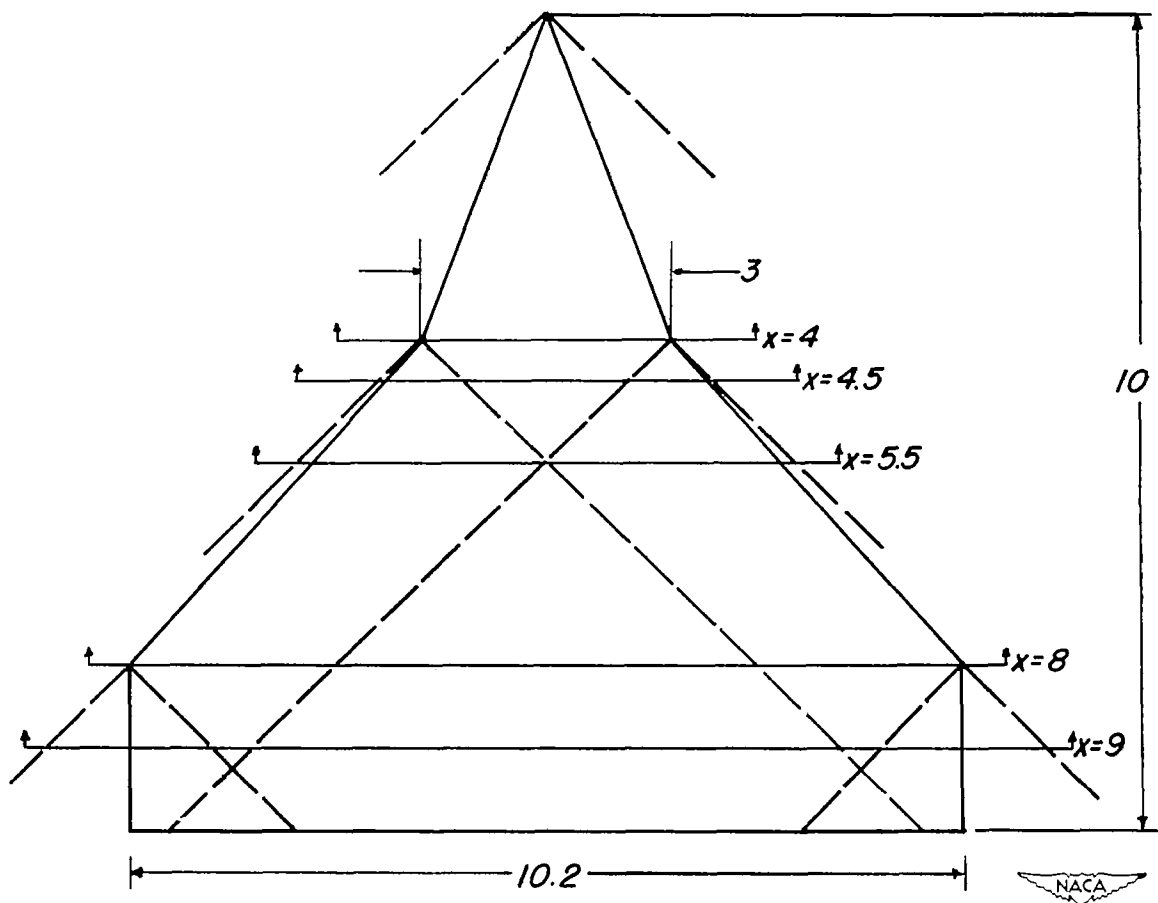


Figure 7.— Plan form of wing for which lift distributions were calculated, and Mach line pattern at $M = 1.414$.

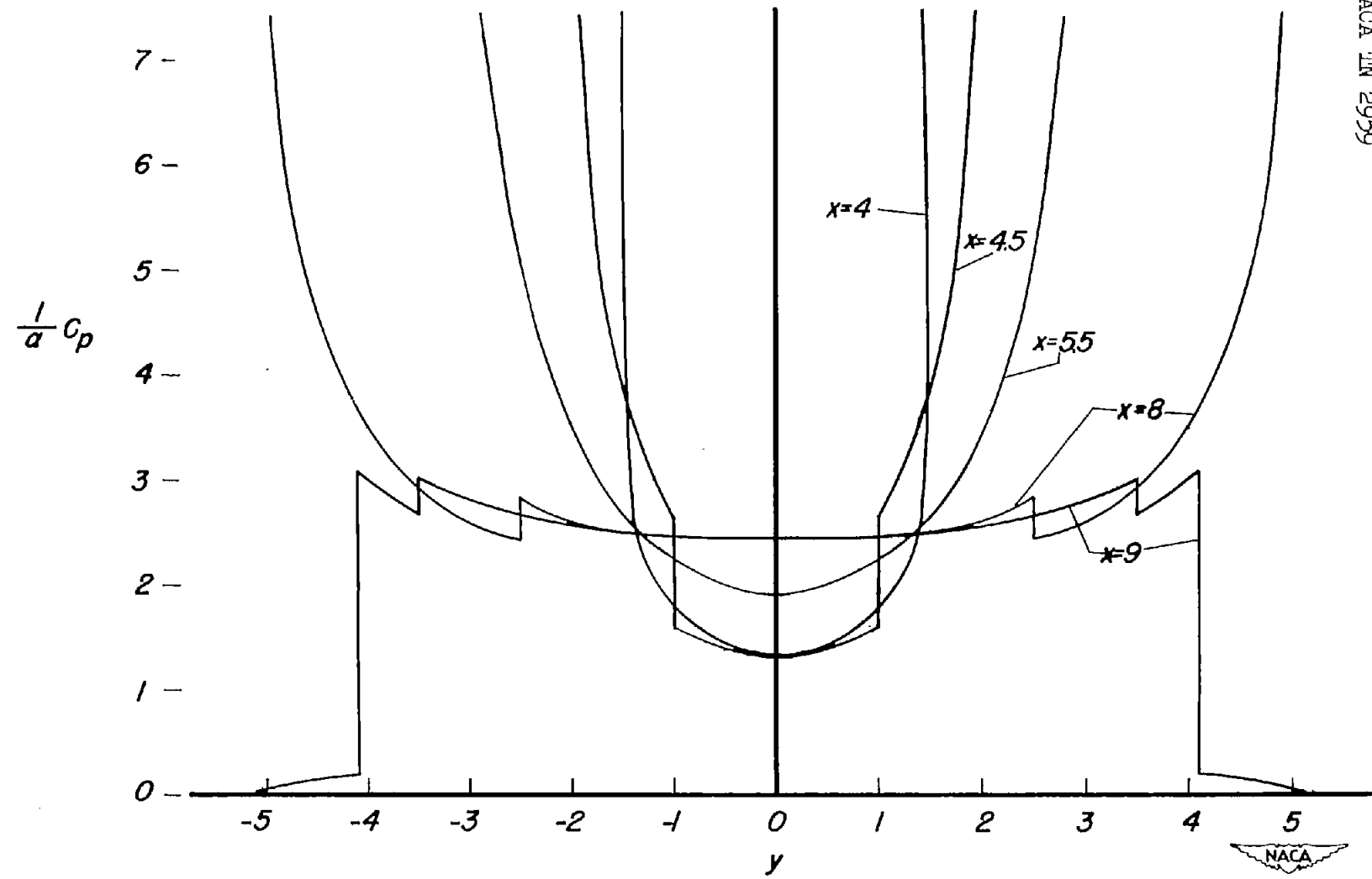


Figure 8.— Spanwise lift distribution at various streamwise stations of wing shown in figure 7,
with $M = 1.414$ ($m_2 < 1$).

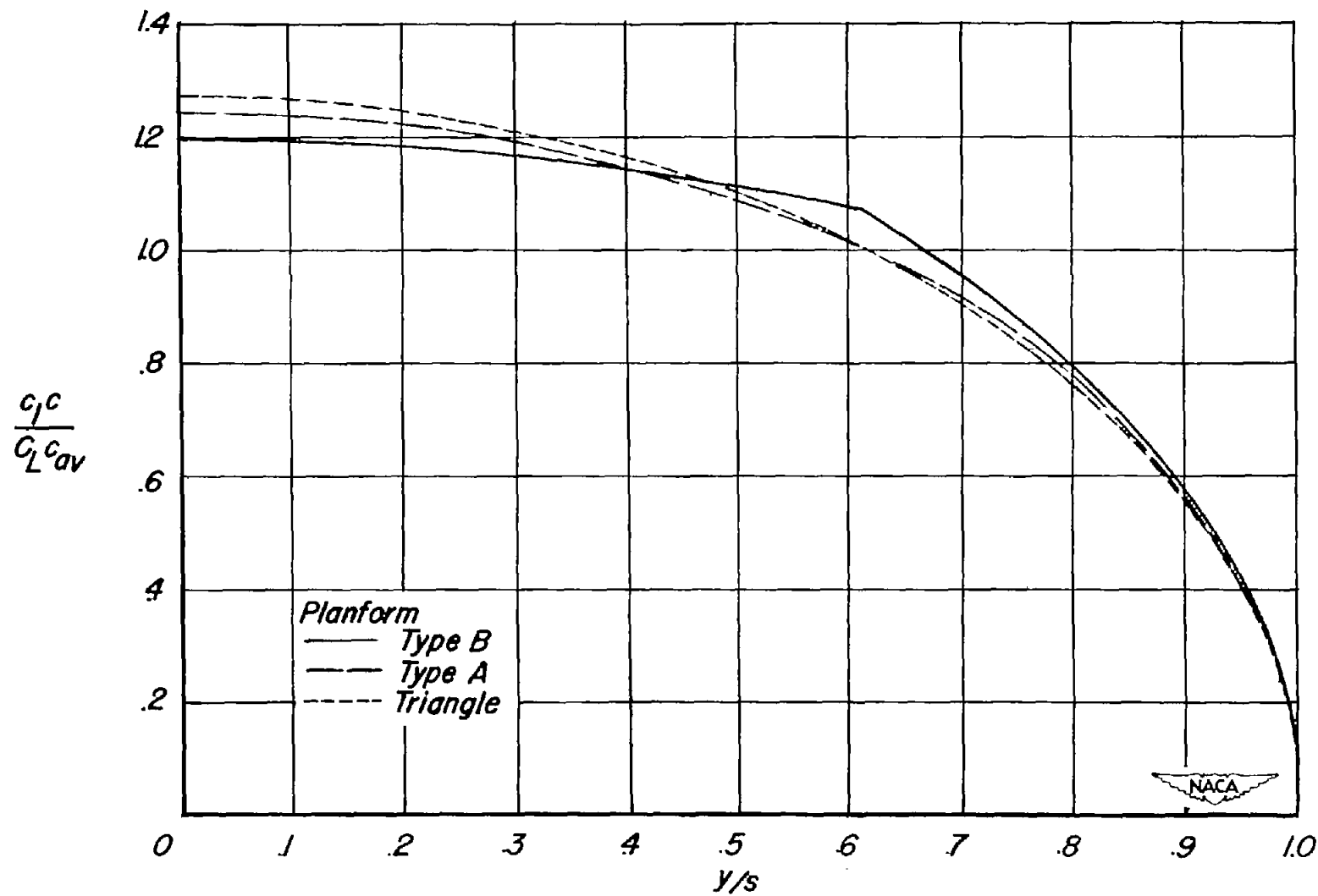


Figure 9.— Span loadings for wing of figure 7 and for type A wing with same leading-edge dimensions, compared with span loading for triangle.

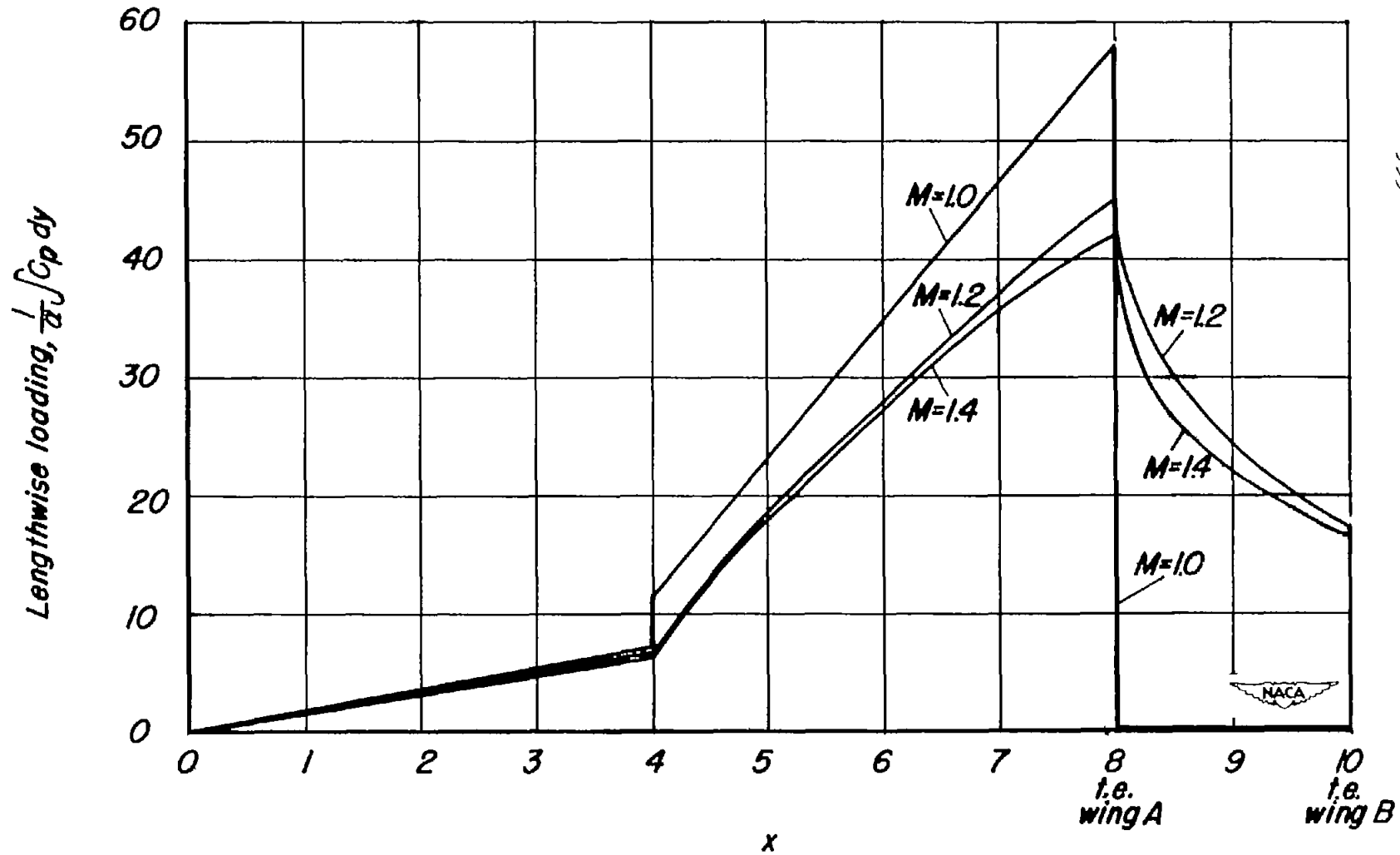


Figure 10.— Lengthwise distribution of load on wing of figure 7 and on type A wing with same leading-edge dimensions at Mach numbers 1.0, 1.2, and 1.4.

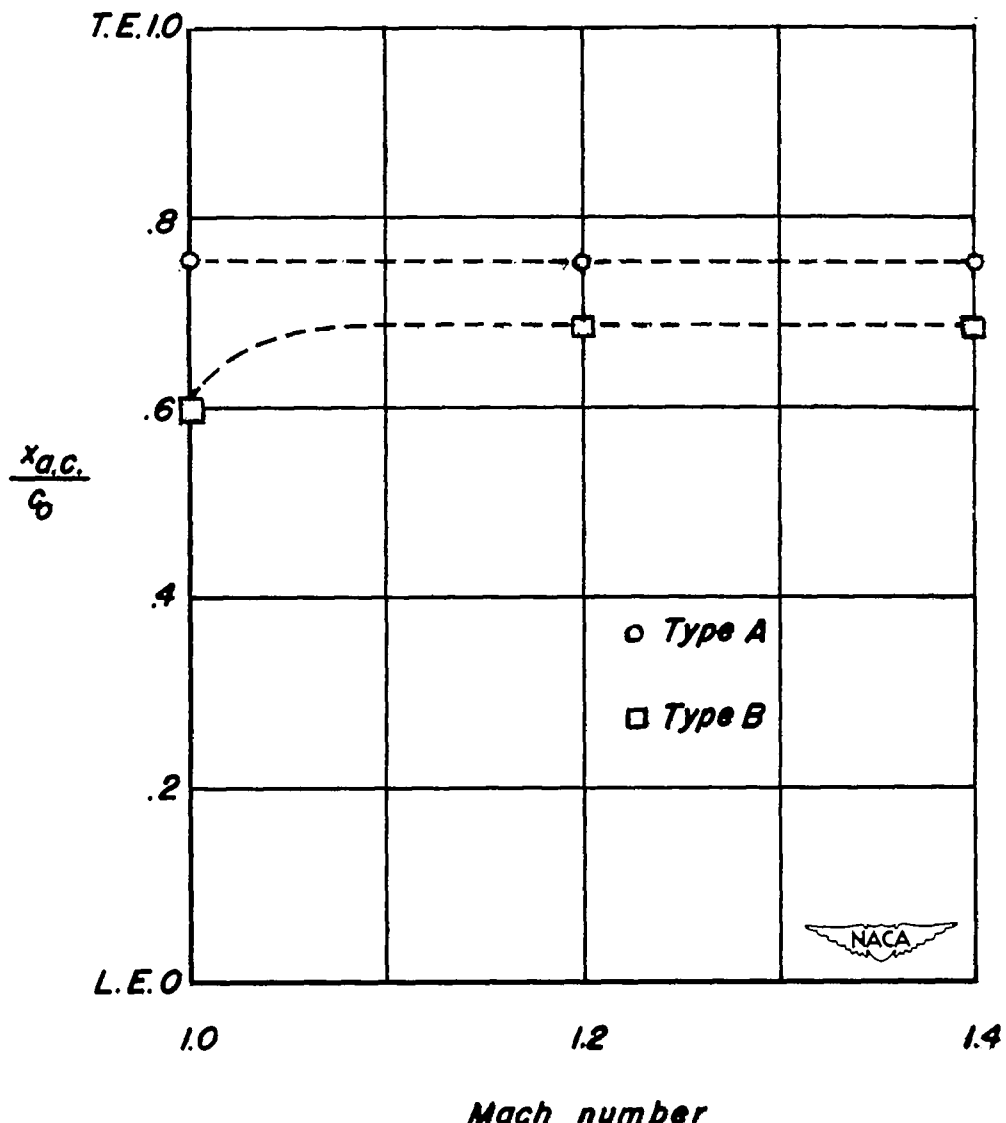


Figure 11.— Variation of aerodynamic-center location with Mach number for wing of figure 7, and for type A wing with same leading edge.

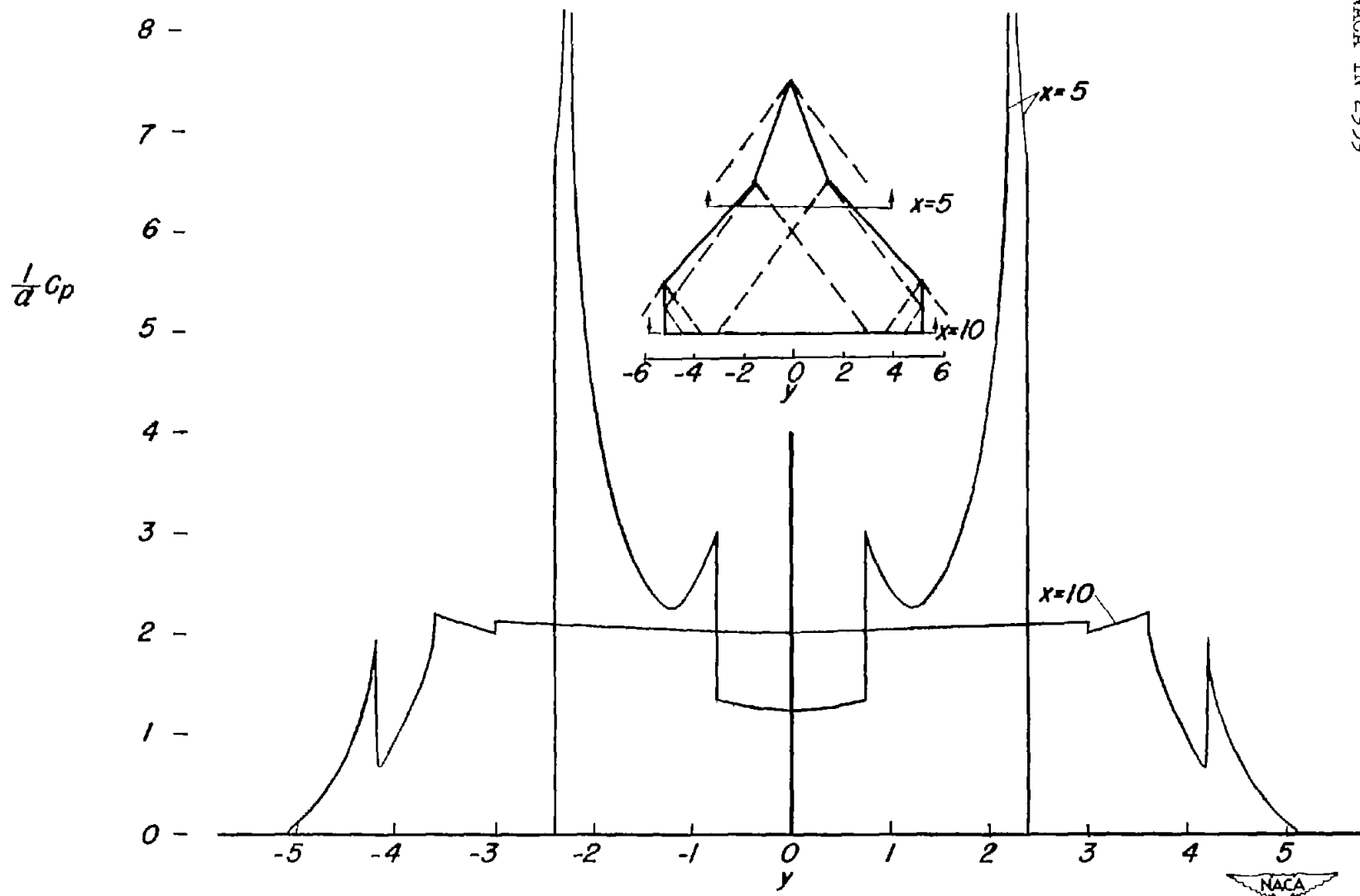


Figure 12.— Mach line pattern and lateral lift distribution at $x = 5$ and $x = 10$ for wing of figure 7, at $M = 1.667$.

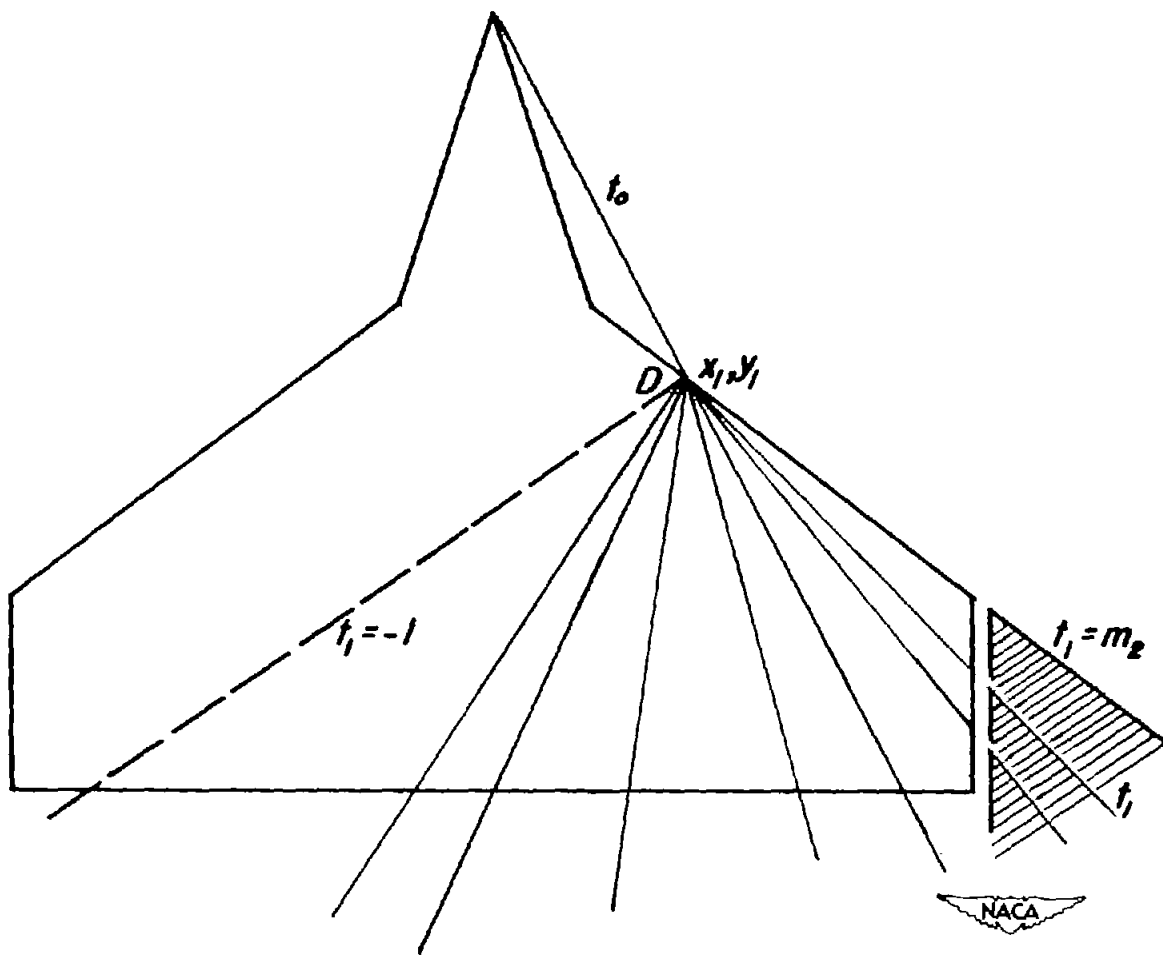
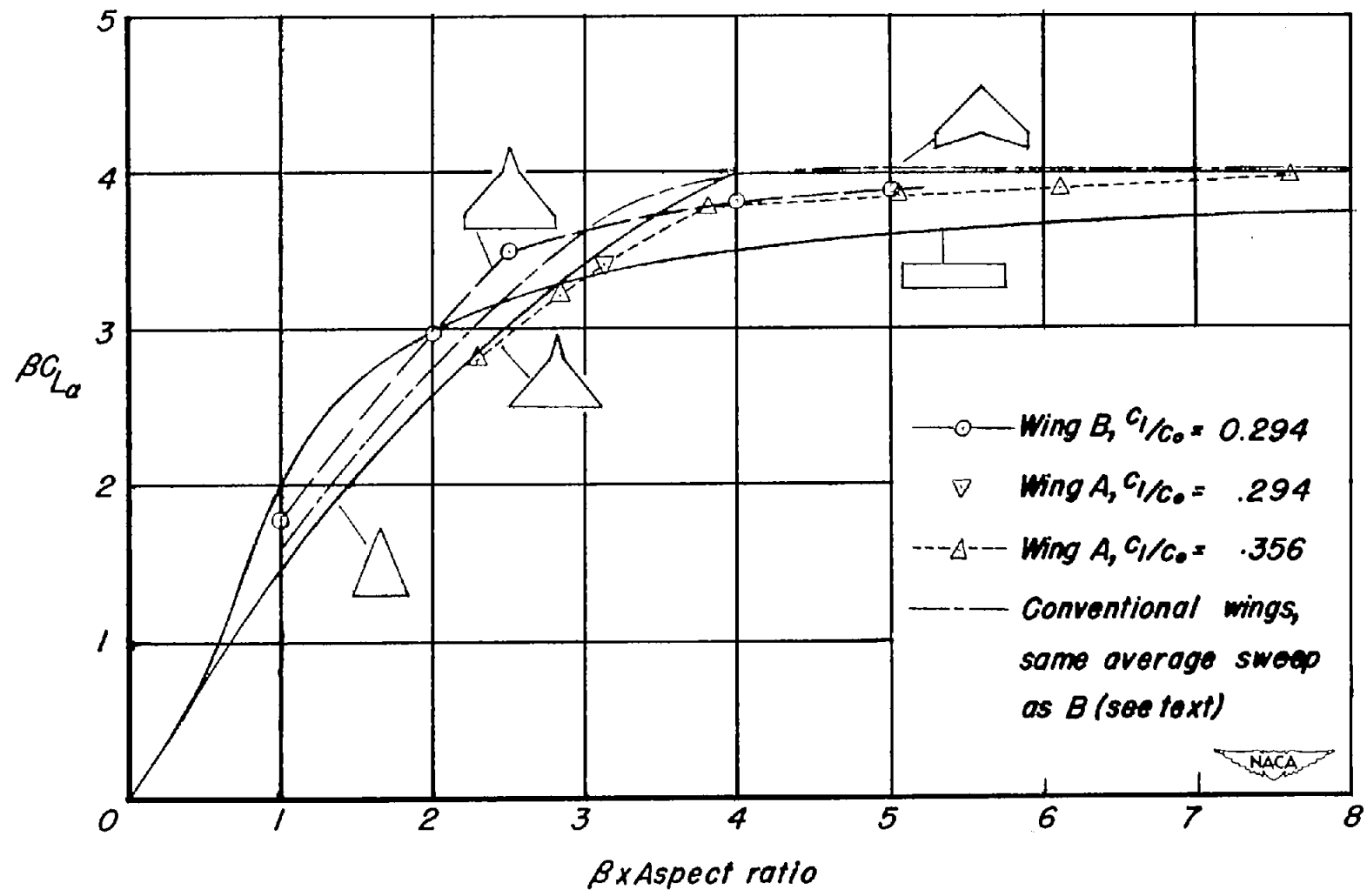
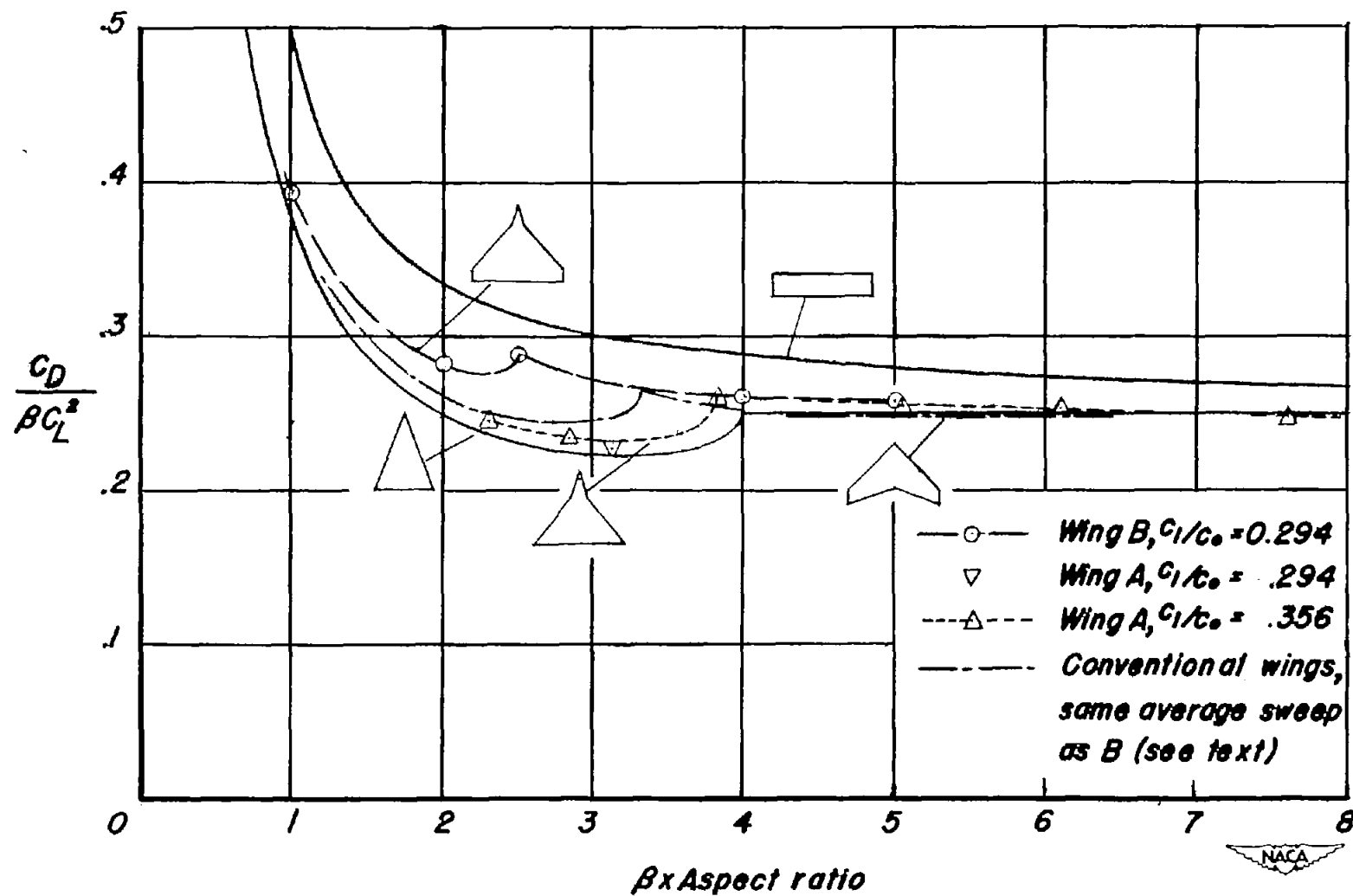


Figure 13.— Method of correcting lift of elementary upwash-cancellation field for tip effect.

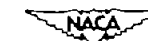


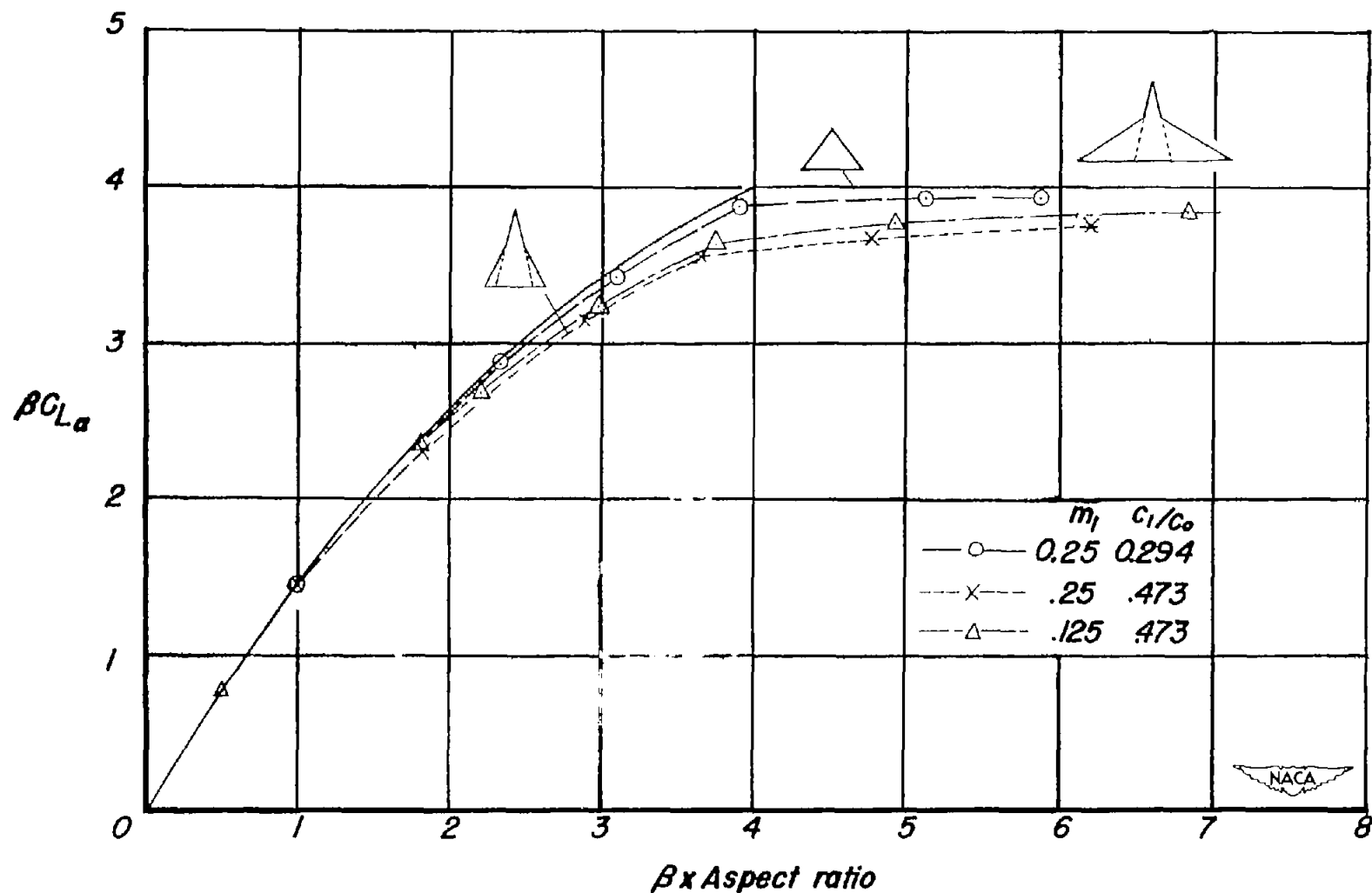
(a) Lift-curve slope.

Figure 14.— Variation of lift-curve slope $\beta C_{L\alpha}$ and drag-rise factor $C_D/\beta C_L^2$ with aspect ratio and Mach number. (Aspect-ratio increase obtained by increasing all spanwise dimensions.) 47



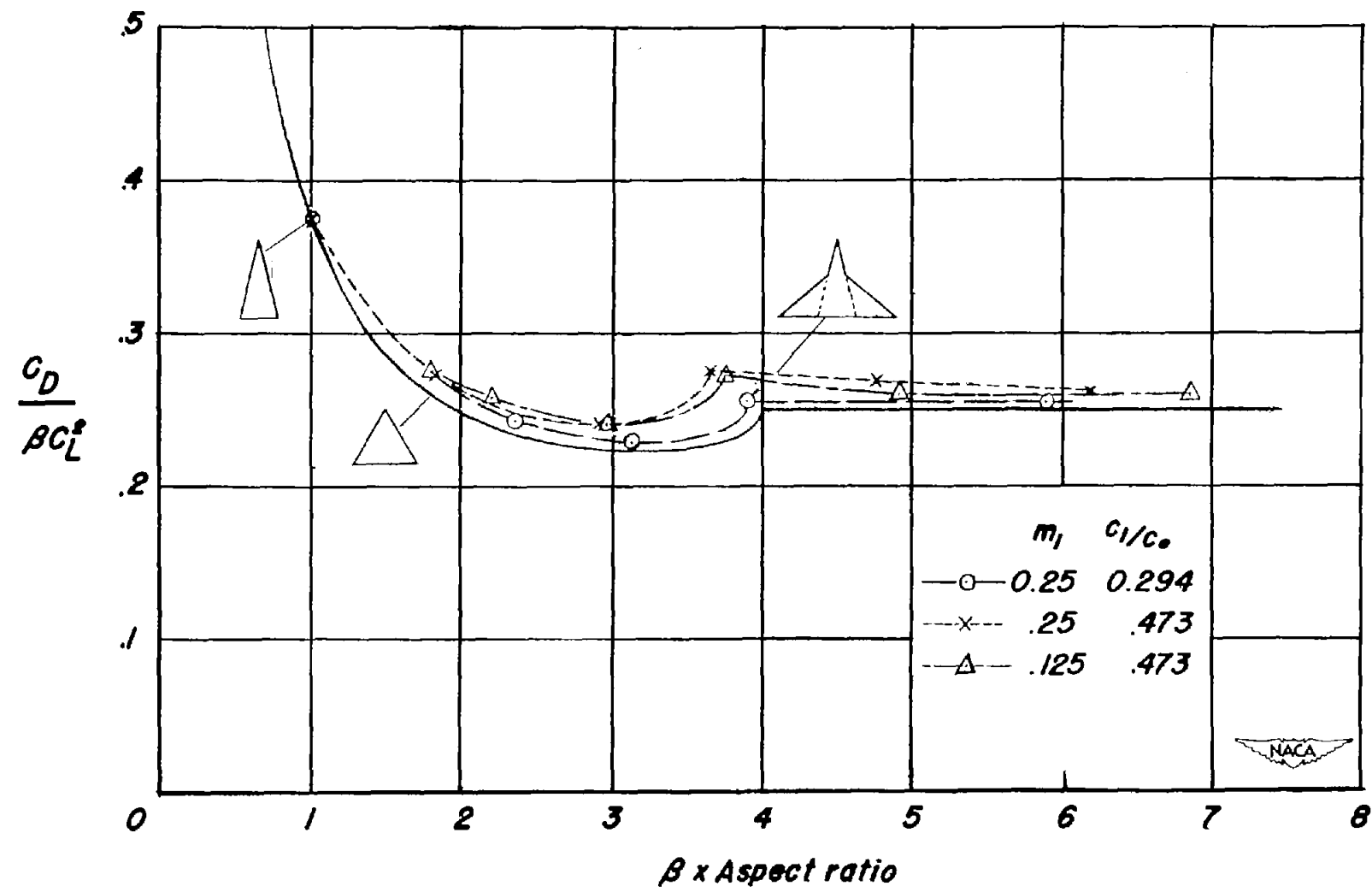
(b) Drag-rise factor.
Figure 14.— Concluded.





(a) Lift-curve slope.

Figure 15.—Effect on βCL_{α} and CD/CL^2 of adding area with reduced sweep at the tips of a triangular wing.



(b) Drag-rise factor

Figure 15.— Concluded.

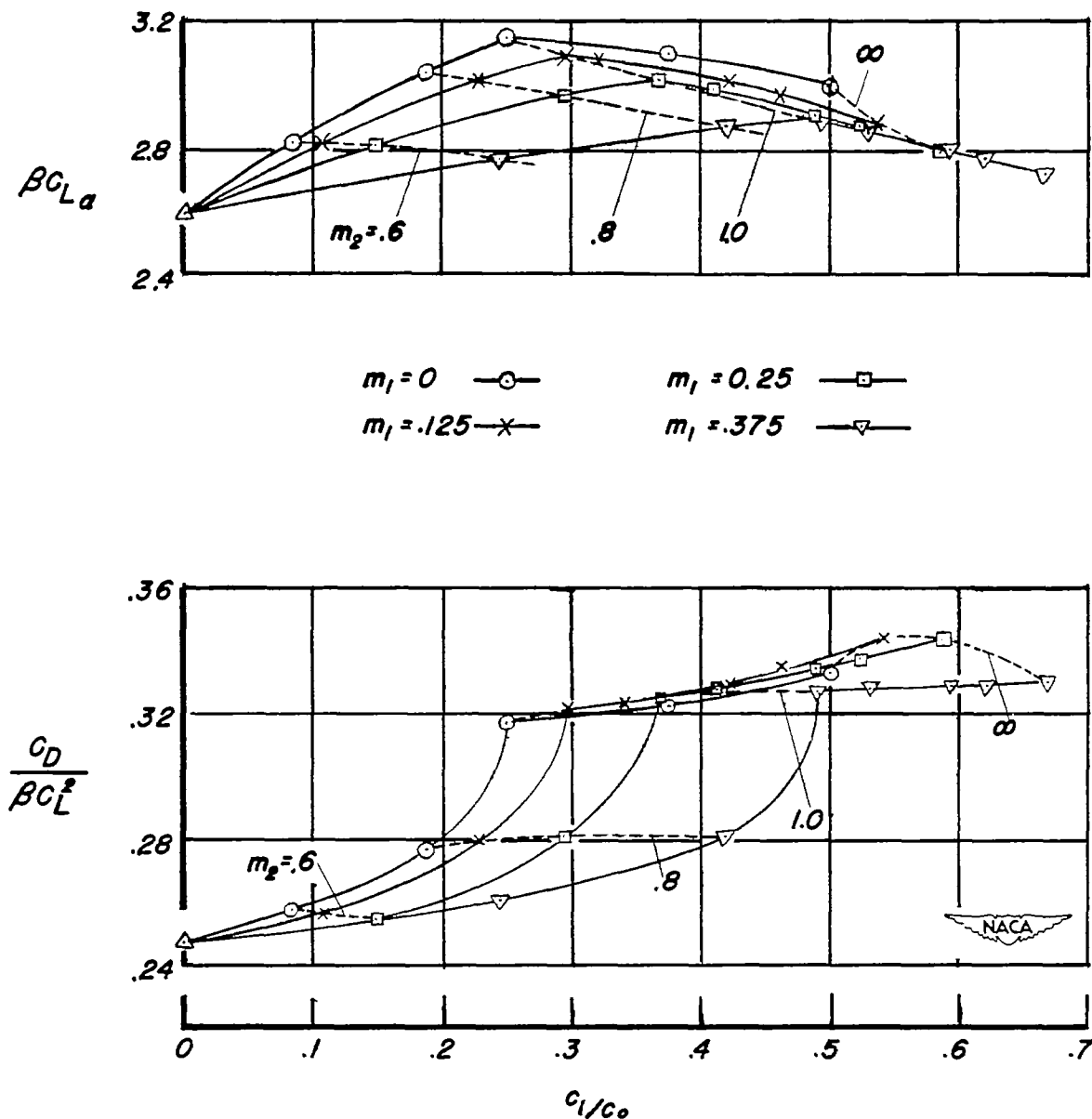


Figure 16.— Variation of $\beta C_{L\alpha}$ and $C_D / (\beta C_{L\alpha}^2)$ with m_1, m_2 and chordwise extent of region of increased sweep; $\beta \times$ aspect ratio = 2.